

**Applied Meteorology Unit (AMU)**  
**Quarterly Report**  
**Second Quarter FY-98**

**Contract NAS10-96018**

**30 April 1998**

**ENSCO, Inc.**  
**1980 N. Atlantic Ave., Suite 230**  
**Cocoa Beach, FL 32931**  
**(407) 853-8105 (AMU)**  
**(407) 783-9735**

## Distribution:

NASA HQ/M-7/S. Oswald  
NASA HQ/Q/F. Gregory  
NASA HQ/M/W. Trafton  
NASA HQ/AS/F. Cordova  
NASA KSC/PH/R. Sieck  
NASA KSC/PH/D. King  
NASA KSC/PH/R. Roe  
NASA KSC/AA-C/L. Shriver  
NASA KSC/AA/R. Bridges  
NASA KSC/MK/D. McMonagle  
NASA KSC/PH-B/J. Oertel  
NASA KSC/PH-B3/T. Greer  
NASA KSC/AA-C-1/J. Madura  
NASA KSC/AA-C-1/F. Merceret  
NASA KSC/BL/J. Zysko  
NASA KSC/DE-TPO/K. Riley  
NASA JSC/MA/T. Holloway  
NASA JSC/ZS8/F. Brody  
NASA JSC/MS4/W. Ordway  
NASA JSC/MS4/R. Adams  
NASA JSC/DA8/J. Bantle  
NASA MSFC/EL23/D. Johnson  
NASA MSFC/SA0-1/A. McCool  
NASA MSFC/EL23/S. Pearson  
45 WS/CC/D. Urbanski  
45 WS/DOR/W. Tasso  
45 WS/SY/D. Harms  
45 WS/SYA/B. Boyd  
45 RANS/CC/S. Liburdi  
45 OG/CC/P. Benjamin  
45 MXS/CC/J. Hanigan  
45 LG/LGQ/R. Fore  
CSR 1300/M. Maier  
CSR 4140/H. Herring  
45 SW/SESL/D. Berlinrut  
SMC/CWP/D. Carroll  
SMC/CWP/J. Rodgers  
SMC/CWP/T. Knox  
SMC/CWP/R. Bailey  
SMC/CWP (PRC)/P. Conant  
Hq AFSPC/DDOR/G. Wittman  
Hq AFSPC/DRSR/S. Heckman  
Hq AFMC/DOW/P. Yavosky  
Hq AFWA/CC/J. Hayes  
Hq AFWA/DNXT/D. Meyer  
Hq AFWA/DN/L. Freeman  
Hq AFWA/DNXM  
Hq USAF/XOW/F. Lewis  
AFCCC/CCN/M. Adams  
Office of the Federal Coordinator for Meteorological Services and Supporting Research  
SMC/SDEW/B. Hickel  
SMC/MEEV/G. Sandall  
NOAA "W/OM"/L. Uccellini  
NOAA/OAR/SSMC-I/J. Golden  
NOAA/ARL/J. McQueen

NOAA Office of Military Affairs/T. Adang  
NWS Melbourne/B. Hagemeyer  
NWS/SRHQ/H. Hassel  
NWS "W/SR3"/D. Smith  
NSSL/D. Forsyth  
NWS/"W/OSD5"/B. Saffle  
PSU Department of Meteorology/G. Forbes  
FSU Department of Meteorology/P. Ray  
NCAR/J. Wilson  
NCAR/Y. H. Kuo  
30 WS/CC/C. Davenport  
30 WS/DOS/S. Sambol  
30 SW/XP/R. Miller  
NOAA/ERL/FSL/J. McGinley  
SMC/CLNER/B. Kempf  
Aerospace Corp./B. Lundblad  
Tetrattech/NUS Corp./H. Firstenberg  
ENSCO ARS Div. V.P./J. Pitkethly  
ENSCO Contracts/M. Penn

## Executive Summary

This report summarizes AMU activities for the second quarter of FY 98 (January - March 1998). A detailed project schedule is included in the Appendix.

During this quarter, AMU personnel supported six expendable vehicle launches and one Shuttle mission at Range Weather Operations. Mr. Nutter also visited the Spaceflight Meteorology Group (SMG) at Johnson Space Center (JSC) from 20-23 January 1998 to observe weather operations in support of the STS-89 launch. While at JSC, he also conducted a briefing on the status of current AMU tasks.

Dr. Manobianco and Ms. Lambert attended the American Meteorological Society (AMS) Annual Meeting in Phoenix, AZ in January. Ms. Lambert presented results from the 915 MHz profiler wind data QC task at the 10th Symposium on Meteorological Observations and Instrumentation. Dr. Manobianco presented the preliminary results of the wind analyses from the 26-27 July 1997 case at the Second Symposium on Integrated Observing Systems, and selected results from the extended 29-km eta model objective evaluation at the 12th Conference on Numerical Weather Prediction. These meetings provided an opportunity to receive comments and suggestions on our work from other experts in the field and to take advantage of their experiences with similar projects.

Mr. Wheeler completed the report on the evaluation of WSR-88D thunderstorm cell attributes and trends in hail and high wind cases. The report will be distributed in April 1998. Mr. Wheeler also began work on the AMU's SIGMET/IRIS task this quarter. The primary goal of this task is to evaluate the capabilities of the SIGMET/IRIS processor on the WSR-74C radar for meeting the operational requirements of the 45WS and SMG in support of all ground, launch, and landing operations. A summary of the WSR-88D cell trends final report and a description of the SIGMET/IRIS task are given in this report.

Dr. Taylor and Ms. Lambert modified the Median Filter and Weber-Wuertz algorithms to quality control simulated real-time data. They completed the analysis of the routines, and Ms. Lambert began writing the final report on the wind data quality assessment. The report contains descriptions of the profiler network and the algorithms used, and a detailed discussion of their performance in both post-analysis and real-time modes. A description of the quality control routines, a discussion of their results, and a summary of the conclusions are given in this report.

Mr. Evans continued analyzing the plume resulting from the Delta 2 explosion on 17 January 1997 using WSR-88D radar observations and the atmospheric models REEDM, RAMS, and HYPACT. Preliminary results from his analyses are presented in this report. Mr. Evans also continued work on the U.S. Air Force's Model Validation Program (MVP) Data Analysis project. The primary purpose of the MVP is to produce RAMS and HYPACT data for the three MVP sessions conducted at CCAS in 1995-1996. This program involves evaluation of Range Safety's modeling capability using controlled releases of tracers from both ground and aerial sources. The status of the analyses for each session is given in this report.

Mr. Nutter completed the objective evaluation of the meso-eta model and began writing the final report for the task. In this quarter, statistics were generated for several of the warm and cool season convective indices. The error statistics for the convective index forecasts were determined using all available model and observational data in 1996 and 1997. These statistics are presented in this report.

Dr. Manobianco obtained, installed, and tested a new version of ADAS. Recent modifications to ADAS include the addition of a complex cloud analysis scheme and provisions to handle aircraft data, satellite-derived cloud drift and water vapor winds, and other single level data types. Dr. Manobianco also developed, tested, and installed software needed to reformat several other data types into ADAS.

Dr. Merceret continued to advise John Lane, a Ph.D. candidate at the University of Central Florida, on a study of the measurement of raindrop size distributions and their effect on Z-R relations. The work is directed at improving the use of WSR-88D and raingauge data as ground truth for NASA's TRMM project.

## SPECIAL NOTICE TO READERS

AMU Quarterly Reports are now published on the Wide World Web (WWW). The Universal Resource Locator for the AMU Home Page is:

<http://technology.ksc.nasa.gov/WWWaccess/AMU/home.html>

The AMU Home Page can also be accessed via links from the NASA KSC Internal Home Page alphabetical index. The AMU link is "CCAS Applied Meteorology Unit".

If anyone on the current distribution would like to be removed and instead rely on the WWW for information regarding the AMU's progress and accomplishments, please respond to Frank Merceret (407-853-8200, francis.merceret-1@ksc.nasa.gov) or Ann Yersavich (407-853-8203, anny@fl.ensco.com).

### 1. BACKGROUND

The AMU has been in operation since September 1991. The progress being made in each task is discussed in Section 2 with the primary AMU point of contact reflected on each task and/or subtask.

### 2. AMU ACCOMPLISHMENTS DURING THE PAST QUARTER

#### 2.1 TASK 001 AMU OPERATIONS

Mr. Nutter visited the Spaceflight Meteorology Group (SMG) at Johnson Space Center (JSC) from 20-23 January 1998 to observe weather operations in support of the STS-89 launch. Mr. Richard Lafosse (SMG) helped arrange the visit and explained the motivation and methodology behind many of the operational support procedures. Mr. Nutter met with Mr. Frank Brody (SMG) to discuss aspects of SMG operations including organization, responsibilities, and issues associated with forecasting and evaluating Shuttle flight rules at time ranges from 0 to 5 days. While at JSC, he also conducted a briefing on the status of current AMU tasks. The briefing and associated discussions lasted approximately two hours with an audience that included about six to eight SMG staff members. Overall, the visit helped maintain the two-way flow of information between SMG and the AMU by face to face discussions of work that is usually described only through written reports.

#### 2.2 TASK 004 INSTRUMENTATION AND MEASUREMENT

##### SUBTASK 1 NEXRAD EXPLOITATION (MR. WHEELER)

During this quarter Mr. Wheeler completed his report entitled, WSR-88D Cell Trends Final Report. This report will be distributed in May 1998.

The purpose of this report is to document the AMU's evaluation of the Cell Trends display as a tool for radar operators to use in their evaluation of storm cell strength. The objective of the evaluation is to assess the utility of the WSR-88D graphical Cell Trends display for local radar cell interpretation in support of the 45 Weather Squadron (45 WS), SMG, and National Weather Service (NWS) Melbourne (MLB) operational requirements.

The evaluation guidelines along with the selected case days were determined by consensus among the 45 WS, SMG, NWS MLB, and AMU. Four case days for a total of 52 cells were selected for evaluation: 29 March and 23 April 1997 (cold season cases) and 11 July 1995 and 13 August 1996 (warm season cases). The WSR-88D (Level II) base data from the NWS MLB was used along with WATADS (WSR-88D Algorithm Testing and Display) from the National Severe Storm Laboratory (NSSL) as the analysis tool. WATADS allows for the replay of historical data and has all the algorithms used in the WSR-88D Build 9 operational system so it closely matches the WSR-88D PUP product output.

The analysis procedure was to identify each cell and track the maximum reflectivity, height of maximum reflectivity, storm top, storm base, hail and severe hail probability, cell-based Vertically Integrated Liquid (VIL) and core aspect ratio using WATADS Build 9.0 cell trends information. One problem noted in the analysis phase was that the Storm Cell Identification and Tracking (SCIT) algorithm had a difficult time tracking the small cells

associated with the Florida weather regimes. The analysis indicated numerous occasions when a cell track would end or an existing cell would be give a new ID in the middle of its life cycle.

This investigation has found that most cells which produce hail or microburst events have discernible Cell Trends signatures. Forecasters should monitor the PUP's Cell Trends display for cells that show rapid (1 scan) changes in both the height of maximum reflectivity and cell-based VIL. For microburst production, there is generally

- An 8 Kft or greater decrease in the height of maximum reflectivity (initially at 18 Kft or greater) **and**
- A decrease in cell-based VIL by 10 kg/m<sup>2</sup> or greater prior to the wind event.

For the hail events there is generally a rapid (1 volume scan) increase in

- The height of maximum reflectivity by 8 Kft or greater to 18 Kft or greater **and**
- The cell-based VIL by 10 kg/m<sup>2</sup> or greater prior to the hail events.

It is important to note that this a very limited data set (four case days). Approximately 52 storm cells were analyzed during those four days. The probability of detection was 88% for both events. The False Alarm Rate (FAR) was a 36% for hail events and a respectable 25% for microburst events. In addition, the Heidke Skill Score (HSS) was 0.65 for hail events and 0.67 for microburst events. The HSS is 0 for a random forecast and 1 for a perfect forecast.

Radar operators need to monitor storm cells and watch for trends that change quickly. Any quick change in a cell's structure is usually a precursor that a cell characteristic has changed or is changing. These changes can be associated with the development or decay of a severe storm. Using the WSR-88D PUP Cell Trends display can help the forecaster in highlighting trends in a cell's attributes of: maximum reflectivity, height of maximum reflectivity, storm top, storm base, hail and severe hail probability, and cell-based VIL. The AMU found that two of the key attributes to monitor are height of the maximum reflectivity and cell-based VIL. By monitoring these two attributes simultaneously a forecaster can have advance warning that a storm cell is becoming severe and may produce a microburst or hail. A rapid decrease in both attributes may indicate that the cell may have microburst potential and a rapid increase in both attributes may indicate that the cell is a hail producer.

If you would like a copy of this report contact Mr. Wheeler at [markw@fl.ensco.com](mailto:markw@fl.ensco.com).

## **SUBTASK 2 915 MHZ BOUNDARY LAYER PROFILERS (DR. TAYLOR)**

Ms. Lambert attended the American Meteorological Society (AMS) Annual Meeting in Phoenix, AZ the week of 12 January. While at the 10th Symposium on Meteorological Observations and Instrumentation, she presented results from using the consensus time check, the rain contamination check, and the Weber-Wuertz algorithm to assess the quality of the 915 MHz profiler wind data.

Dr. Taylor and Ms. Lambert modified the Weber-Wuertz (WW) algorithm and Median Filter to quality control (QC) simulated real-time data. These algorithms perform both spatial and temporal checks of the data. The post-analysis temporal checks compare data points to those in previous and subsequent profiles. In real-time QC algorithms, the current profile is compared to profiles from previous times only. This test revealed how the algorithms would perform in a real-time, operational setting.

Ms. Lambert began writing the interim report on the wind data quality assessment. The report contains descriptions of the profiler network and the algorithms used, and a detailed discussion of their performance in both post-analysis and real-time modes. The following sections provide descriptions of the algorithms and a brief discussion of the results. Detailed descriptions of the consensus time period, precipitation contamination, and WW algorithms are given in the previous AMU Quarterly Report (First Quarter FY-98). For completeness, summary descriptions of these algorithms are given with detailed descriptions of the post-analysis and real-time WW and Median Filter algorithms.

## *The QC Algorithms*

Four QC algorithms were applied to the data. The consensus time period algorithm, the rain contamination algorithm, WW, and the Median Filter. The WW and Median Filter algorithms underwent modifications in order to simulate real-time QC. Descriptions of the algorithms and the modifications needed to simulate real-time performance are given in the following paragraphs.

### **Consensus Time Period Check**

When a profiler is reset during a consensus period, all data collected up to the time of the reset is erased. However, the profiler will continue to collect data through the end of the allotted period and calculate a consensus wind. If the reset occurs toward the end of the period, a consensus wind is calculated from data collected over a very short time period. This tends to create erroneous wind profiles. If a profile is calculated from a consensus period of less than 6 minutes, it is flagged as suspect. No modifications were needed for this algorithm to be used in real time.

### **Rain Contamination Check**

It is well documented that rain can contaminate 915 MHz profiler data and is manifested in the data as large downward vertical velocities and high signal-to-noise ratios (SNRs) (Ralph et al. 1996). Strong downward velocities and high SNRs in the data sets were often associated with erroneous profiles when rain was reported over the Cape area. Plots of SNR versus vertical velocity revealed two distinct populations separating clear-air and rain contaminated data points. This allowed development of a discriminant function (Panofsky and Brier 1968) which is used to determine if a wind estimate is contaminated by rain. No modifications were needed for this algorithm to be used in real time.

### **Weber-Wuertz Algorithm**

The Weber-Wuertz algorithm (WW) will recognize patterns in one- or two-dimensional arrays of any desired data type. It is currently set up to recognize patterns in time and space in the individual consensus radial velocities of the three beams used in the consensus. WW requires that certain parameters be set that dictate how the program will establish patterns. Several iterations of tests were done using several data sets to determine the appropriate settings. The next two sections describe the post-analysis and real-time versions of WW.

#### *Post-Analysis Mode*

Although any time period can be used, in this study WW checks 24 hours of data at a time in post-analysis mode. This was convenient because each file contains 24 hours of data, which equates to 3072 points (96 profiles X 32 gates). All the data are input to the routine, then the patterns are determined for the whole period. Thus, data collected before and after the wind estimate in question is used to determine whether or not the estimate fits into a pattern.

#### *Real-Time Mode*

When used in real time, this routine will only check the data in the current profile for reliability. WW will only have present and past data available to check for continuity. Simulations using archived data sets give an indication of the performance that can be expected from using WW in real time.

The technique used in this study is similar to that used in Barth et al. (1997). It uses a sliding time window to establish patterns, then checks all data points in the time window but only retains the results for the current profile. WW must establish new patterns when a new profile is introduced and uses a sliding window in order to use a consistent time period over which patterns are established. The QC information from the previous profiles is retained when establishing new patterns, i.e. wind estimates previously flagged by WW and any other routine within the current time window are not used to quality control the current profile. The time period chosen must be large enough for the algorithm to establish legitimate patterns, yet be small enough to allow the algorithm enough time to process the data before the next profile arrives and so that the current profile is displayed in a timely manner. After several tests a time period of 6 hours, or 25 profiles, was chosen.

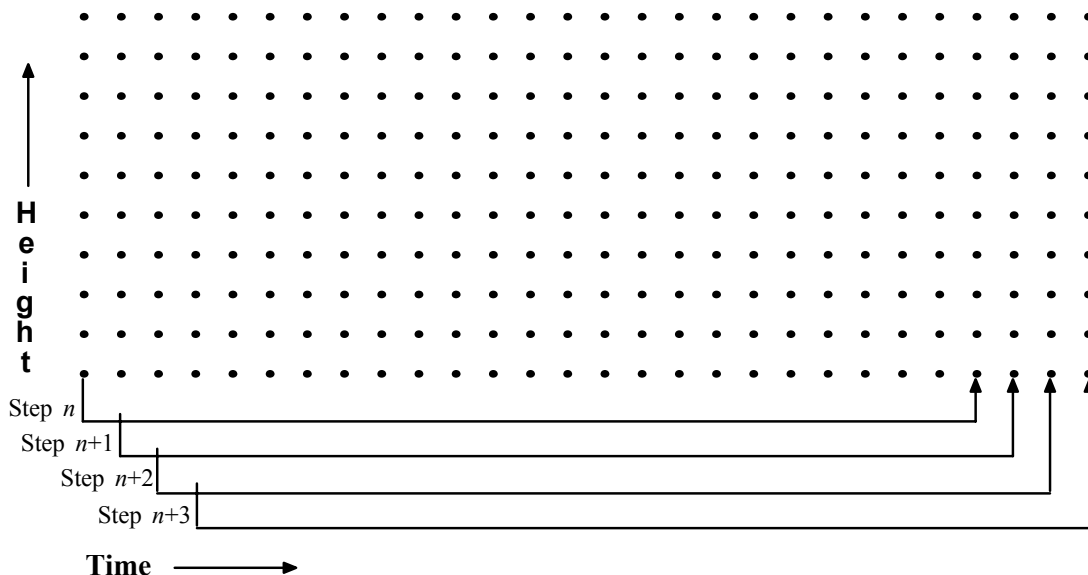


Figure 1. Illustration of the method in which WW is operated in real-time mode. The dots indicate the time-height data points, the four brackets below the grid labeled Step  $n$ , Step  $n+1$ , and so on represent the sliding time window, and the arrows on the right hand side of the brackets point to the current profile being QC'd.

In Fig. 1 a grid of dots representing a portion of the data in each of the profiles over 28 time periods is shown. The first bracket, labeled Step  $n$ , encompasses the 25 profiles used in WW to establish data patterns. These patterns are used to QC the current profile, which is indicated by the arrow on the right-hand side of the bracket. Suspect data are flagged in this profile alone during this step. When a new profile is produced, the window slides to the right, as shown by the bracket labeled Step  $n+1$ , and new patterns are established in WW as the process is repeated.

**Median Filter**

The median filter described in this section is not related in any form to the Median Filter/First Guess (MFFG) algorithm (Wilfong et al. 1993) which is used only on the NASA 50-MHz DRWP data. The MFFG is applied to the individual beam spectral data as a temporal filter to remove outliers. The median filter in this study uses equations that are adaptations of the routines developed in Carr et al (1995). It tests the temporal and spatial consistency of the u- and v-components of the calculated horizontal wind in an attempt to identify suspect data. The reader should not attempt to relate the performance of the MFFG to the performance of WW based on the comparisons of the median filter and WW algorithms contained in this section.

This algorithm compares the u- and v-components of a horizontal wind observation to the medians of the u- and v-components of the surrounding (space and time) observations. If the difference between the observed wind component,  $u_i$  and/or  $v_i$ , and the median of the neighboring observations,  $u_m$  and/or  $v_m$ , exceeds a critical threshold,  $T_u$  and/or  $T_v$ , then the wind observation,  $u_i$  and  $v_i$ , is flagged as suspect.

The critical threshold values,  $T_u$  and  $T_v$ , are computed as follows:

$$T_u = \max(T_{u1}, T_2) \text{ and}$$

$$T_v = \max(T_{v1}, T_2)$$

where

$$T_{u1} = 0.2 * |u_m + u_i|,$$

$$T_{v1} = 0.2 * |v_m + v_i|, \text{ and}$$

$$T_2 = a * (A * h^2 + B * h + C).$$

In  $T_2$ ,

- a = 1.3,
- h = height of the wind observation (feet),
- A =  $-5.695 \times 10^{-9}$ ,
- B =  $3.66 \times 10^{-4}$ , and
- C = 7.3834.

The next two sections describe the post-analysis and real-time versions of the Median Filter.

**Post-Analysis Mode**

For each wind observation the number of unflagged wind observations,  $N$ , in the eight surrounding points in a  $3 \times 3$  space and time grid box (30 minutes X 200 m) is determined (Fig. 2). If  $N$  is greater than 3, then the medians of the  $u$ - and  $v$ -components of the unflagged wind observations are calculated and the median filter test is performed.

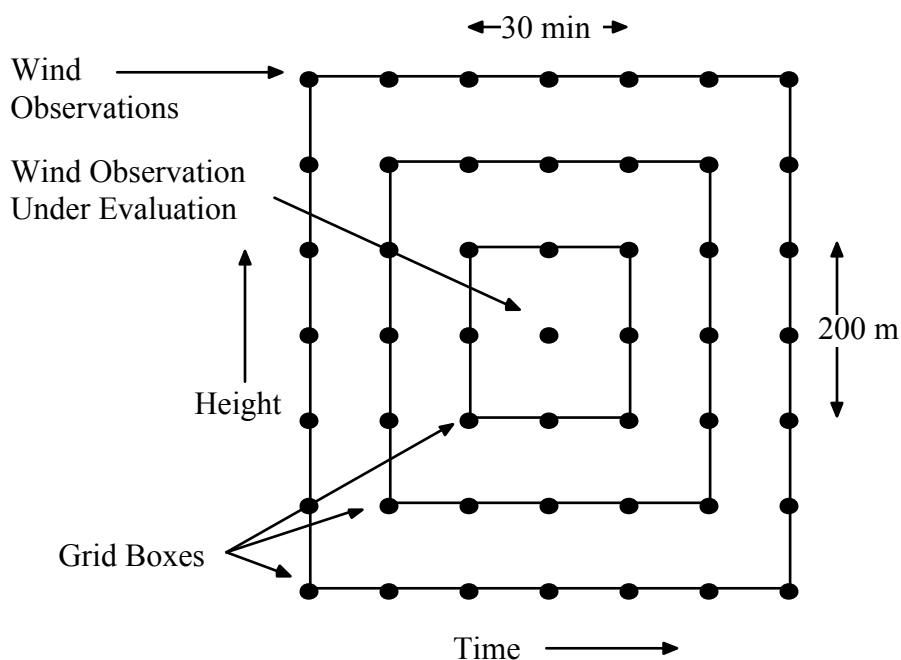


Figure 2. Illustration of the method in which the median filter is operated in post-analysis mode. The dots indicate the time-height wind observations and the center dot is the observation being QC'd.

If  $N$  is less than 3, then the test grid box is enlarged to a  $5 \times 5$  space and time grid box (1 hour X 400 m) and the same test procedure is invoked. If  $N$  is greater than 3 for the 24 surrounding points in the  $5 \times 5$  grid box, then the medians of the  $u$ - and  $v$ -components of the unflagged wind observations are calculated and the median filter test is performed. If  $N$  is still less than 3 for the  $5 \times 5$  grid box, then the test grid box is enlarged to a  $7 \times 7$  space and time grid box (1.5 hours X 600 m) and the same test procedure is invoked. If  $N$  is greater than 3 for the 48 surrounding points in the  $7 \times 7$  grid box, then the medians of the  $u$ - and  $v$ -components of the unflagged wind observations are calculated and the median filter test is performed. If  $N$  is less than 3 for the  $7 \times 7$  grid box, then the median filter test is not applied and that wind observation is not flagged.

**Real-Time Mode**

For each wind observation, the number of unflagged wind observations,  $N$ , in the five surrounding points in a  $3 \times 2$  space and time grid box (15 minutes X 200 m) is determined (Fig. 3). Note that in real-time mode the grid box is not symmetrical since the reference wind observations must be from the current or previous time periods. If  $N$  is

greater than 3, then the medians of the u- and v-components of the unflagged wind observations are calculated and the median filter test is performed.

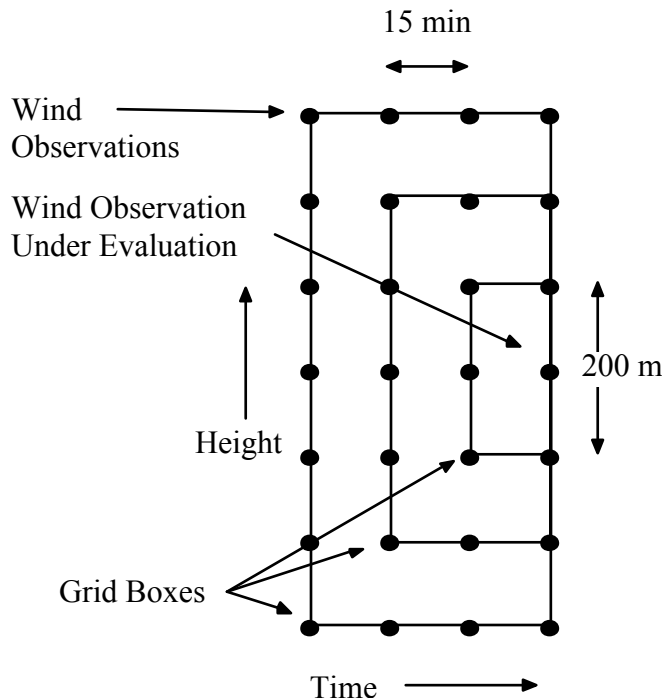


Figure 3. Illustration of the method in which the median filter is operated in real-time mode. The dots indicate the time-height wind observations and the dot at right-center is the observation being QC'd.

If N is less than 3, then test grid box is enlarged to a 5x3 space and time grid box (30 minutes X 400 m) and the same test procedure is invoked. If N is greater than 3 for the 14 surrounding points in the 5x3 grid box, then the medians of the u- and v-components of the unflagged wind observations are calculated and the median filter test is performed. If N is still less than 3 for the 5x3 grid box, then the test grid box is enlarged to a 7x4 space and time grid box (45 minutes X 600 m) and the same test procedure is invoked. If N is greater than 3 for the 27 surrounding grid points in the 7x4 grid box, then the medians of the u- and v-components of the unflagged wind observations are calculated and the median filter test is performed. If N is less than 3 for the 7x4 grid box, then the median filter test is not applied and that wind observation is not flagged.

**Routine Combinations**

No one routine is able to effectively flag suspect data when used on its own. Combinations of the four routines were examined, and two of those combinations were found most effective:

Combination 1 (CPW)

- Consensus Time
- Precipitation Contamination
- Weber-Wuertz

Combination 2 (CPM)

- Consensus Time
- Precipitation Contamination
- Median Filter

The precipitation contamination and consensus time routines were used in both combinations. Both of these routines were very effective at flagging data that met the specific criteria of each routine. The median filter and WW routines were used in the combinations to flag all other suspect wind estimates.

The algorithms must be used in a certain order. The consensus time period and rain contamination checks do not depend on time or space continuity of the data, but only on the data values associated with the wind estimate being checked. They are used to QC the data first to remove the obviously bad wind estimates. This ensures that

WW will not see the areas of bad data as legitimate patterns and that the median filter will not use the bad values in the calculation of the median values. When run in the order shown in the above lists, the algorithms do very well in flagging most of the bad data points while flagging few good data points.

### **Data**

Profiler data for this study were collected during the period 1 May through 31 August 1997. Five days with different weather phenomena were chosen from this period for algorithm development and testing. They are summarized in Table 1. The use of data collected in diverse weather conditions allows for a thorough analysis of how the routines respond in different weather regimes.

Table 1. Summary of case days and their associated weather phenomena.	
<i>Date</i>	<i>Meteorological Conditions</i>
2 May 1997	Dry conditions, afternoon sea breeze
12 May 1997	Rain over network all day
15 May 1997	Nocturnal jet, afternoon sea breeze
18 May 1997	Convection near network, afternoon sea breeze
17 June 1997	Nocturnal jet, convection over network, afternoon sea breeze

### **Results**

Results of the post-analysis and real-time modes of the CPW and CPM combinations are given in the next two sections. All the data sets listed in the previous section were used in both the post-analysis and real-time versions of the two combinations. Since they needed modification to run in real-time, the consensus time period and precipitation contamination checks flagged the same wind estimates in both modes and in both combinations. The differences in the results are entirely due to the differences between the Median Filter and WW.

#### **Post-Analysis Mode**

The median filter and WW performed similarly in number of wind estimates flagged on most days. However, there is large difference on 12 May in which WW flagged 140 more wind estimates than the median filter. The bulk of this difference can be explained in the way both algorithms treat areas of isolated data. In the case of the median filter, if there are not enough wind estimates to determine a median value, the wind estimate is not flagged. However, if a pattern contains less than 32 wind estimates, WW will flag all wind estimates in that pattern. This can occur in areas where there are small groups of wind estimates surrounded by many missing (or previously flagged) winds. The WW algorithm can not connect these isolated groups with other patterns in the data. After the precipitation contamination algorithm was run in the 12 May data, such small pockets of isolated data existed.

This is best illustrated by comparing Figs. 5 and 6 (Fig. 4 contains the raw wind speed data). In Fig. 5 there are some data left by CPM between 0600 and 0800 UTC at 2000'. CPW identified these isolated consensus winds as patterns with less than 32 wind estimates and flagged them as suspect. There are other areas of data seen as vertical lines at 1200, 1645, 2015, and 2130 UTC in Fig. 5 that are not seen in Fig. 6 for this reason.

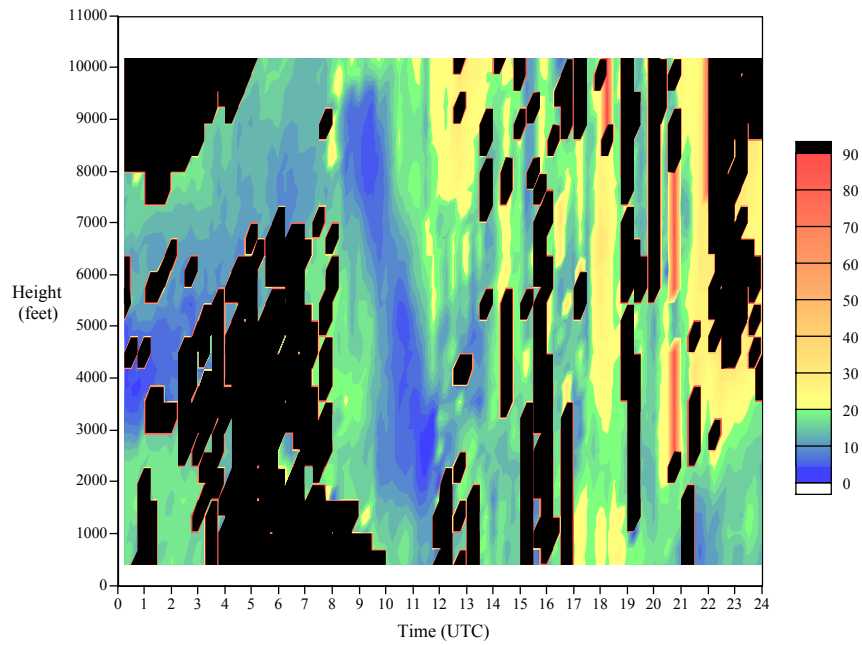


Figure 4. Wind speeds from the False Cape profiler on 12 May 1997. Speeds are in knots (legend at right). Areas of black indicate gates where a consensus wind was not calculated. Precipitation contamination can be seen in the data mainly as temporally inconsistent wind speeds from profile to profile after 0800 UTC.

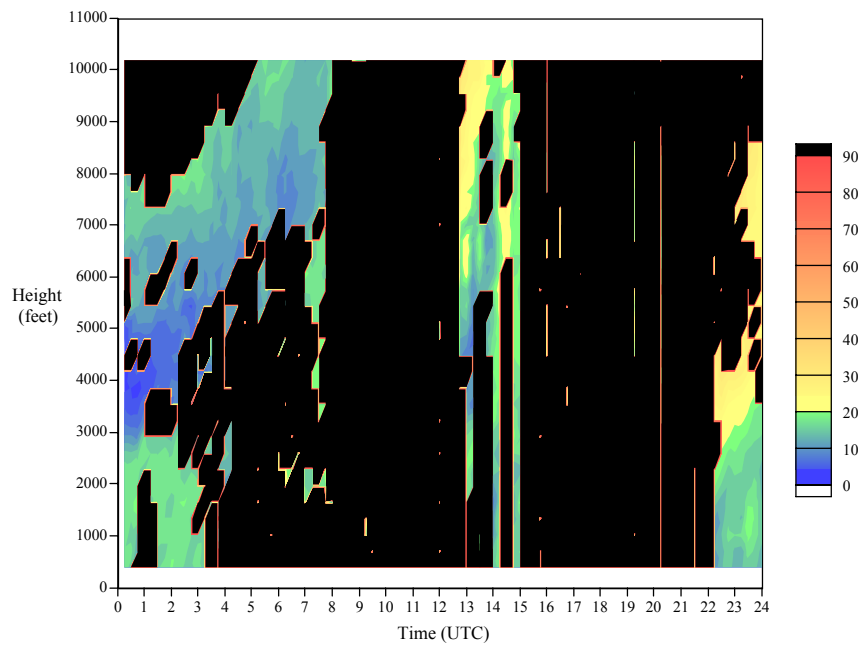


Figure 5. Wind speeds from the False Cape profiler on 12 May 1997 after CPM. Speeds are in knots (legend at right). Areas of black indicate gates where a consensus wind was not calculated and where the data were flagged by the algorithms.

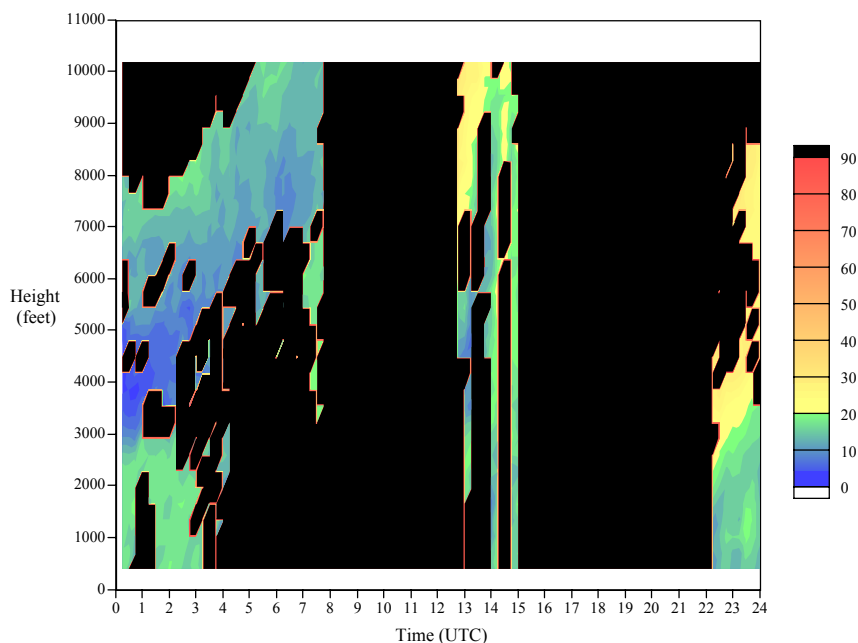


Figure 6. Wind speeds from the False Cape profiler on 12 May 1997 after CPW. Speeds are in knots (legend at right). Areas of black indicate gates where a consensus wind was not calculated and where the data were flagged by the algorithms.

#### Real-Time Mode

A large difference in the number of wind estimates flagged between CPW and CPM on 12 May also existed in real-time mode. The cause of this difference is the same as that for post-analysis mode and is discussed in the previous section. A new large difference in the number of wind estimates flagged between CPW and CPM appeared on 17 June. The raw wind speeds are shown in Fig. 7, and Figs. 8 and 9 show the wind speeds after CPM and CPW, respectively. The large difference in the number of wind estimates flagged can be found mainly in the two profiles at 1815 and 2000 UTC.

CPW flagged the two complete profiles at 1815 and 2000 UTC (Fig. 9). Most of the winds were flagged because they did not fit the patterns that existed before the missing wind profiles. CPM did not flag any wind estimates in the 1815 UTC profile, and flagged 11 wind estimates in the 2000 UTC profile between 4000 - 5500', 7500 - 8500', and the top-most wind estimate (see white arrows in Fig. 8). At 1815 UTC the missing data affected CPM such that it would only have the data above and below a wind estimate in the same profile to calculate the median (see Fig. 3). The winds in this profile were spatially consistent at all levels and none were flagged. This was not the case for the profile at 2000 UTC. Substantially stronger values from the 1915 UTC profile were used in the calculation of the medians for the 2000 UTC wind estimates causing several of the wind estimates at this time to be flagged. CPW flagged two complete profiles in which CPM only flagged 11 wind estimates. This accounts for most of the difference in the number of wind estimates flagged between the two combinations on 17 June.

Note that CPW did not flag the 6 wind estimates at 2030 UTC between 6500 - 8500' (see white arrow in Fig. 9). These data are obviously erroneous and should have been flagged. The entire profile at 2030 UTC was affected by rain and all other wind estimates in the profile were flagged by the precipitation contamination algorithm. The data in question were not flagged by the precipitation contamination algorithm because it will not flag wind estimates in which less than 60% of the individual beam estimates were used in the calculation of the consensus vertical velocity. WW will also not flag a wind estimate based on an inconsistent vertical velocity if less than 60% of the estimates were used in its calculation. The oblique beam consensus velocities fit into previous patterns in WW and, therefore, the wind estimates were not flagged by this algorithm. The horizontal wind estimates, however, are highly inconsistent with the estimates in the previous profiles. Therefore, CPM successfully flagged these erroneous estimates because the difference between their u- and v-components and the median u- and v-components exceeded the threshold value in the median filter routine.

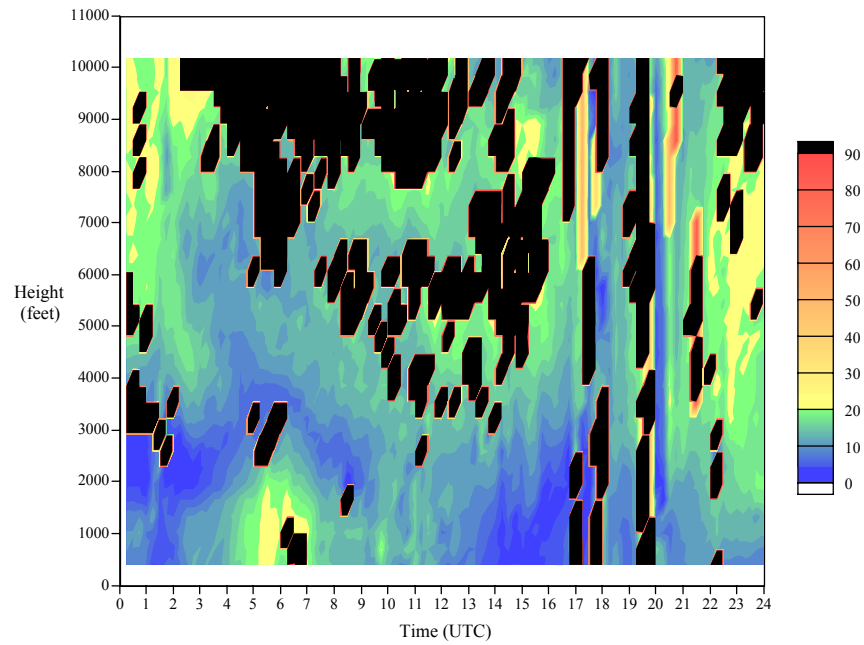


Figure 7. Wind speeds from the False Cape profiler on 17 June 1997. Speeds are in knots (legend at right). Areas of black indicate gates where a consensus wind was not calculated.

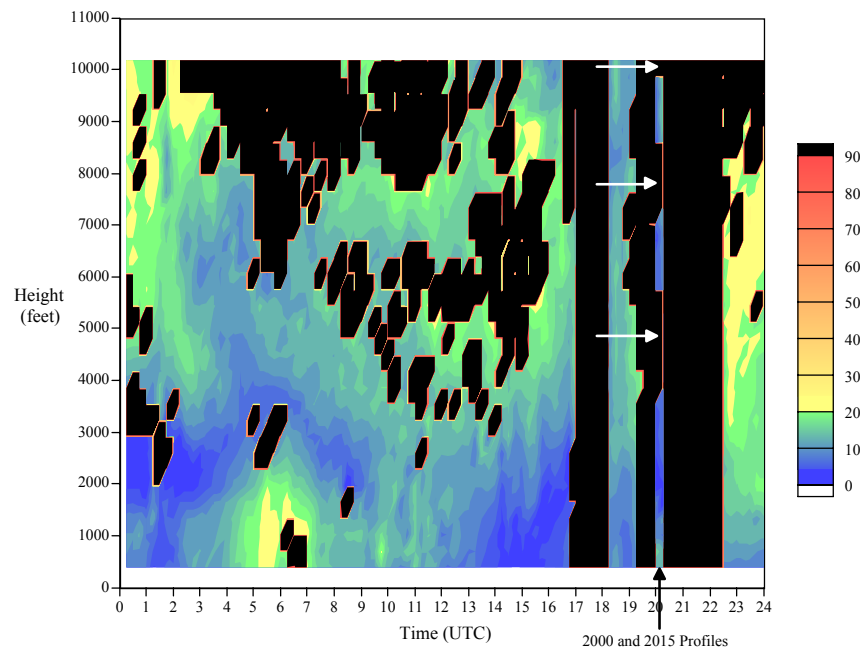


Figure 8. Wind speeds from the False Cape profiler on 17 June 1997 after real-time CPM. Speeds are in knots (legend at right). Areas of black indicate gates where a consensus wind was not calculated and where the data were flagged by the algorithms.

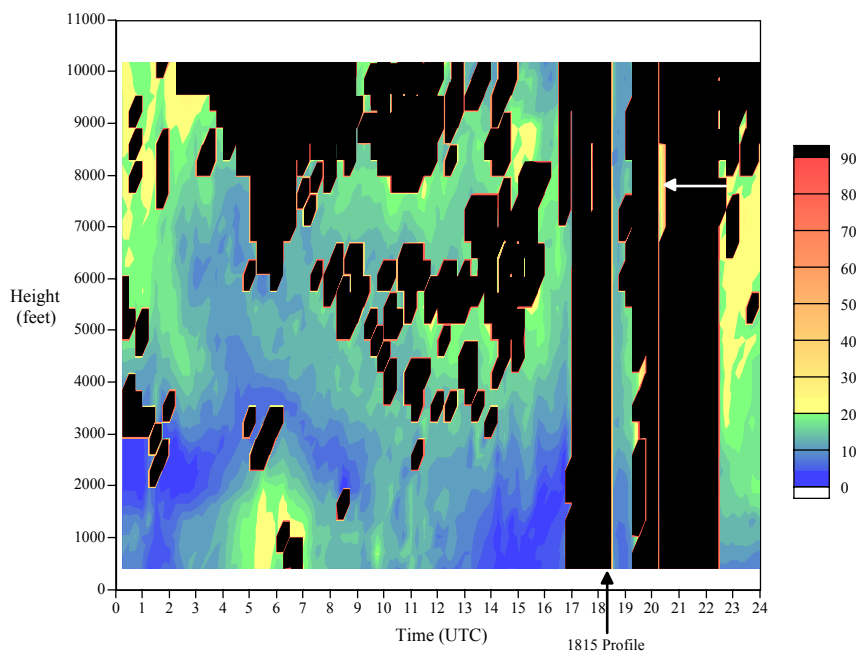


Figure 9. Wind speeds from the False Cape profiler on 17 June 1997 after real-time CPW. Speeds are in knots (legend at right). Areas of black indicate gates where a consensus wind was not calculated and where the data were flagged by the algorithms.

### Summary

The two routine combinations designated as CPM and CPW are compared in post-analysis and real-time modes. Both routines perform similarly in both modes with some notable differences that have been discussed in this section. These differences indicate that CPW is the better routine combination when used in the post-analysis mode, while CPM performs better in the real-time mode.

Care should be taken when choosing one of the routines over the other, however, as they were closely scrutinized on only five 24-hour data sets. An important point to consider is that the median filter was newly modified in the AMU and has not been tested on many data sets, while WW was developed several years ago (Weber and Wuertz 1991) and has been widely tested and used in the profiler community. In light of the small data set used in the analysis and the fact that the results from the median filter were only slightly better than WW in the simulated real-time mode, it is difficult to recommend one routine over the other. Either routine could be used in real time. Whichever routine is chosen, it is critical that the consensus time and precipitation contamination checks be used to flag the obviously bad wind estimates before using either of the dependent routines. Neither the median filter or WW performed acceptably when used alone.

Detailed descriptions of the routines, the data sets, and the results are given in the interim report. This report will be available after external review is complete, which is anticipated to be in May 1998. For a copy of the interim report, please contact Ms. Lambert at [winnie@fl.ensco.com](mailto:winnie@fl.ensco.com).

### References

- Barth, M. F., R. B. Chadwick, and W. M. Faas, 1997: The Forecast Systems Laboratory Boundary Layer Profiler Data Acquisition Project. *First Symposium on Integrated Observing Systems*, Long Beach, CA. Amer. Meteor. Soc., 130 - 137.
- Panofsky, H. A., and G. W. Brier, 1968: *Some Applications of Statistics to Meteorology*. The Pennsylvania State University, 224 pp.

Ralph, F. M., P. J. Neiman, and D. Ruffieux, 1996: Precipitation identification from radar wind profiler spectral moment data: vertical velocity histograms, velocity variance, and signal power - vertical velocity correlations. *J. Atmos. Oceanic Technol.*, **13**, 545-559.

Weber, B.L., and D. B. Wuertz, 1991: Quality control algorithm for profiler measurements of winds and temperatures. NOAA Tech. Memo. ERL WPL-212, 32pp.

Wilfong, T. L., S. A. Smith, and R. L. Creasy, 1993: High temporal resolution velocity estimates from a wind profiler. *J. Spacecraft and Rockets*, **30**, 348-354.

#### **SUBTASK 5 I&M AND RSA SUPPORT (DR. MANOBIANCO/MR. WHEELER)**

During February, Mr. Wheeler reviewed several documents (slides) from Hughes (RSA) on the RWO Weather Display system.

#### **SUBTASK 12 SIGMET/IRIS PROCESSOR EVALUATION (MR. WHEELER)**

The SIGMET/IRIS task was started in January 1998. The primary goal of this task is to evaluate the capabilities of the SIGMET Integrated Radar Information System (IRIS) processor on the WSR-74C radar for meeting the operational requirements of the 45 WS and SMG in support of all ground, launch, flight operations, and Shuttle landings.

For this task, the AMU will collect data and perform a preliminary evaluation of the new SIGMET radar display system for operational use. Specific areas of investigation will include:

- Integrated Reflectivity for Lightning Nowcasting:
  - Investigate the integrated reflectivity in the 0 to -10°, 0 to -20° and -10 to -20° ranges to determine if there are any key signatures that can be used to aid in nowcasting lightning
- Integrated Reflectivity/Echo Tops for Microburst Nowcasting:
  - Investigate IRIS products/alerts of Vertically Integrated Liquid (VIL) and Storm Echo Tops and develop a nomogram threshold table (if possible) as a useful microburst warning tool
- Layered Products for Monitoring Cloud Development:
  - Develop and investigate how best to utilize SIGMET layered products. If useful, these products will be used to monitor cloud development in support of launch and landing operations.
- Product Evaluation and Utilization in Support of Ground and Launch Operations along with Evaluation of Shuttle Flight Rules:
  - Evaluate the capabilities of the system relative to forecaster responsibilities to determine recommendations for optimal use of the system

After the completion of all the analyses, the AMU will document the results, including any recommendations for operational use of the system, in a final report to be delivered in January 1999.

Mr. Wheeler continues to work with the system to gain a better understanding of the SIGMET system. System checkout includes new product generation, testing different product schedules, and archiving and restoring data for playback. In addition, raw data will be archived for spring storms.

Additional memory was added to the AMU's SIGMET/IRIS processor during March. This solved the problem of the system crashing every time more than one display window is opened on the screen. With the additional memory, the system is more robust and does allow more windows to be opened for product display.

### 2.3 TASK 005 MESOSCALE MODELING

#### SUBTASK 4 DELTA EXPLOSION ANALYSIS (MR. EVANS)

The Delta Explosion Analysis project is being funded by KSC under AMU option hours. The primary goal of this task is to conduct a case study of the explosion plume using the RAMS and REEDM models and compare the model results with available meteorological and plume observations. The Melbourne WSR-88D radar data was preliminarily analyzed and provided information on the track of the clouds following the explosion.

The comparison of the observed and predicted plumes is ongoing. Some preliminary results are presented in Fig. 10. The location of the observed plume was determined from the WSR-88D analysis. The location of the predicted plume was determined by analyzing the concentrations predicted by the ERDAS HYPACT model for 10-minute periods from 1630 UTC until 2030 UTC. For each 10-minute period, the maximum concentration in each 75-m thick layer was found. The latitude, longitude, and height of this maximum concentration was then noted.

The graph in Fig. 10 shows the location of the maximum concentration of the layer centered on 412.5 m. This layer is near the center of the ground-based layer which contained the lower plume resulting from the explosion. The plume originated at Launch Complex 17 and then moved south over the following 4 hours. The observed and predicted plume locations closely agreed for the first two hours except that the observed plume was slightly west of the predicted plume. During the last two hours of the model simulation, the graph gives the appearance of a widely spreading plume. This spread was not due to the plume shifting from the east to the west but due to the shift in the location of the predicted maximum concentration within the plume from one 10-minute period to the next.

Figure 11 shows the rawinsonde sounding from 1613 UTC, approximately 15 minutes prior to the explosion. The base of the sharp capping inversion is evident at 900 meters. The bulk of the plume was trapped below this inversion and was advected to the south by the northerly winds in this layer.

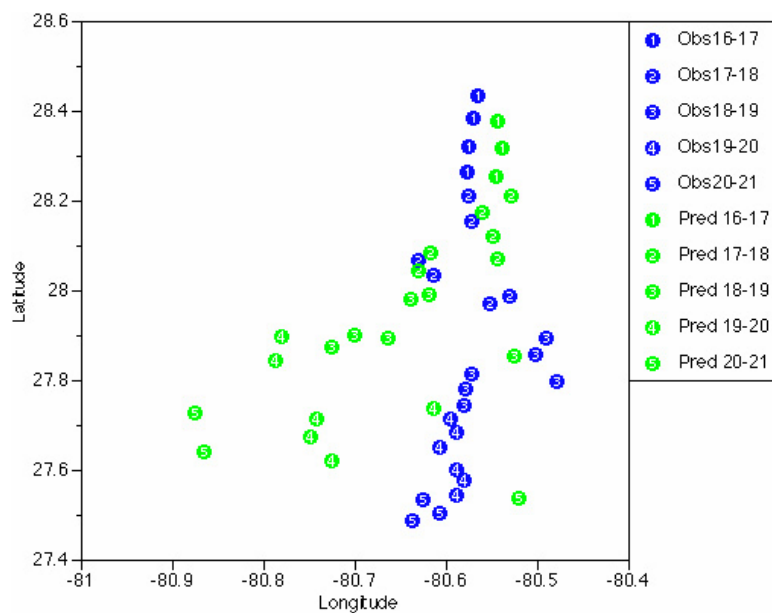


Figure 10. Preliminary data of observed vs. predicted plume location for plume resulting from Delta II explosion at 1628 UTC on 17 January 1997. The observed plume location was determined by WSR-88D radar. The predicted plume location was determined by finding the maximum predicted HYPACT concentration in the 75-m layer centered at a height of 412 m. The numbered circles represent the time of the observed and predicted plumes with the following time tags: 1: 1600-1700 UTC, 2: 1700-1800 UTC, 3: 1800-1900 UTC, 4: 1900-2000 UTC, 5: 2000-2100 UTC.

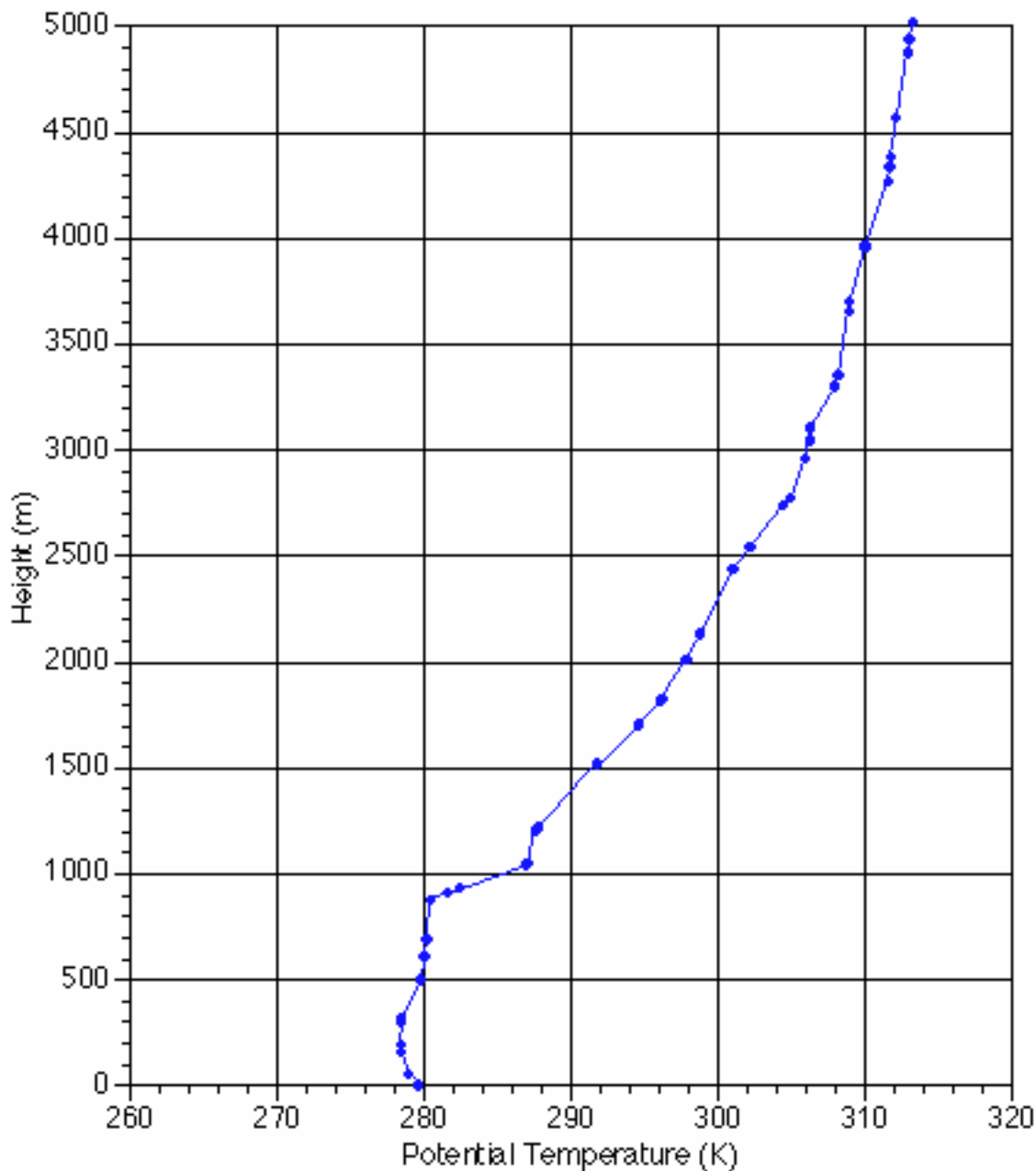


Figure 11. Potential temperature plot of the Cape Canaveral rawinsonde at 1613 UTC on 17 January 1997. Note the strong inversion base at 900 m.

#### **SUBTASK 5 MODEL VALIDATION PROGRAM (MR. EVANS)**

The primary purpose of the U.S. Air Force's Model Validation Program (MVP) Data Analysis project, which is being funded by option hours from the U.S. Air Force, is to produce RAMS and HYPACT data for the three MVP sessions conducted at Cape Canaveral in 1995-1996. This program involves evaluation of Range Safety's modeling capability using controlled releases of tracers from both ground and aerial sources.

The status of the MVP data analysis tasks is presented in Table 2.

Table 2. Status of MVP Data Analysis Tasks

<b>MVP Data Analysis Task</b>	<b>Session I</b>	<b>Session II</b>	<b>Session III</b>
<b>Prepare Data</b>	Completed	In process	Completed
<b>Run ERDAS-RAMS</b>	Completed	Partially completed	Completed
<b>Run ERDAS-HYPACT</b>	In process	To be done	Completed
<b>Run PROWESS-RAMS</b>	Completed	To be done	Completed
<b>Run PROWESS-HYPACT</b>	Completed	To be done	Completed
<b>Submit Data to NOAA-ATDD</b>	To be done	To be done	In process

We continue working on the problem of providing readable tapes of the MVP data to NOAA/ATDD. Apparent incompatibilities between AMU and NOAA tape drives have caused problems but NOAA plans to purchase a tape drive similar to one connected to an AMU PC. This problem should be resolved soon.

Processing of the Session II data is in progress. Nine of the 16 MVP days had missing NGM data (used to initialize RAMS and provide boundary conditions). An alternate source for the missing data is being pursued.

## SUBTASK 6 EXTEND 29-KM ETA MODEL OBJECTIVE EVALUATION (MR. NUTTER)

Data collection for surface and upper-air forecasts and observations at Cape Canaveral Air Station (XMR), Tampa Bay (TBW), and Edwards Air Force Base (EDW) concluded at the end of January 1998. Also in January, Dr. Manobianco presented selected results from this work at the 12th Conference on Numerical Weather Prediction in Phoenix, AZ. Mr. Nutter presented the same information to SMG personnel while visiting JSC to observe weather support for the STS-89 launch. In February, Mr. Nutter completed data quality control and generated verification statistics for the 1997 cool season.

Dr. Manobianco and Mr. Nutter completed preparation of a two-part *Weather and Forecasting (WAF)* manuscript based on meso-eta evaluation results. The manuscript for part I describes results from the objective verification of surface and upper-air point forecasts at XMR, TBW, and EDW. The analysis considers the most recently updated data from both the twin warm (May - August) and cool (October - January) season periods during 1996 and 1997. The manuscript for part II highlights results from the subjective evaluation of the meso-eta model during the 1996 warm and cool seasons. The manuscripts were submitted to the chief editor of *WAF* in March 1998.

In March, Mr. Nutter began working on the final report for this task which will include and expand upon the results presented in part I of the *WAF* manuscript. As an example of the expanded material, a preliminary analysis of meso-eta forecast accuracy for convective parameters is presented in the following sections. Occasional references are made to an earlier verification of upper-air forecast accuracy that was discussed in the previous AMU Quarterly Report (First Quarter FY-98; hereafter QR1-98).

### *Overview*

The meso-eta model configuration and data collection procedures applied for this work are described in QR1-98. Forecast errors are shown here for several warm and cool season convective indices at XMR and TBW. Results for EDW are not shown because convection is usually not a concern at that location. Convective indices are computed using the numerical algorithms in the GEneral Meteorological PAcKage (GEMPAK; desJardins et al. 1997). The characteristics of the forecasts, observations, and their relationship are described using conditional quartile diagrams (Murphy et al. 1989). Forecast errors are additionally quantified using the bias, RMS error, and error standard deviation statistics. The error statistics for the convective index forecasts are determined using all available data in 1996 and 1997 from both the 0300 UTC and 1500 UTC model runs and corresponding observations.

### *Conditional Quartile Diagrams*

Although traditional statistics such as the bias and RMS error are useful for quantifying overall forecast accuracy within a particular sample of data, they fail to describe completely the character of the relationship between given forecasts and their corresponding observations. Murphy et al. (1989) demonstrate that such relationships are revealed, in part, by considering a factorization of the joint distribution between forecasts ( $f$ ) and their observations ( $x$ ). Given a set of data containing  $f$  and  $x$ , the joint distribution  $p(f,x)$  specifies the relative frequency of occurrence for particular combinations of  $f$  and  $x$ . The factorization for the joint distribution considered here is  $p(f,x) = p(x|f)p(f)$ , where  $p(f)$  is the marginal distribution of the forecasts and  $p(x|f)$  is the conditional distribution of the observations given the forecasts. Given the set of available forecasts,  $f$ , the marginal distribution  $p(f)$  describes the relative frequency of occurrence for each forecast value (or discretized range of values). The conditional distribution of the observations given the forecasts,  $p(x|f)$ , specifies the marginal distribution of the subset of all observations  $x$  which correspond to a particular forecast.

The factorization of  $p(f,x)$  is useful because  $p(x|f)$  and  $p(f)$  specify the calibration and refinement of the forecasts, respectively (Murphy et al. 1989). A set of forecasts is perfectly calibrated if, for each forecast  $f$ , the mean observation is equal to  $f$ . A set of forecasts is completely unrefined if the same forecast value is produced on each occasion. Therefore, a set of forecasts may be considered well refined and reliable if the marginal distribution of forecasts  $p(f)$  covers an appropriate range of values and the average of the conditional distribution of observations is equal to the forecast,  $f$ .

The relationship between  $p(x|f)$  and  $p(f)$  may be interpreted graphically using a conditional quartile diagram (Murphy et al. 1989). For each set of convective index forecasts, the marginal distribution of the forecast values,  $p(f)$ , is displayed using histograms. In addition, the conditional distribution of the observations,  $p(x|f)$ , is summarized for each given forecast value by the median, interquartile range (IQR), and minimum and maximum values. The median represents the middle value of a set of ordered data and is alternately called the 50th percentile or 2nd quartile. Similarly, the IQR represents the difference between the 3rd and 1st quartiles (75th and 25th percentiles). The quartile lines extend across those index values that are forecast on at least five occasions and have been smoothed using a simple 3-point hanning algorithm (Tukey 1977). Deviations of the conditional medians from the 45° reference line reveal that the forecasts are conditionally biased. Specifically, deviations above (below) this line indicate forecasts from a particular category, which are more often smaller (larger) than observed. More generally, the diagrams utilize five data points (minimum, 1st, 2nd and 3rd quartiles, and maximum) to describe the character of the conditional distributions for the observations associated with each given forecast value.

Although the terminology is complex, the conditional quartile plots aid operational users by serving as a kind of historical lookup diagram which helps visualize the relationship between given forecasts and observations. For example, if the meso-eta model provides a precipitable water (PWAT) forecast of 30 mm at XMR during the warm season, Fig. 12a indicates that such a forecast is traditionally uncommon and conditionally unbiased, and that 50% of the observations (i.e., the IQR) were within about  $\pm 5$  mm of that given forecast value.

The conditional quartile diagrams presented in Figs. 12-19 describes the relationship between forecast and observed convective indices during both warm and cool season at XMR and TBW. Unless stated otherwise, the discussion refers jointly to the qualitative error characteristics at both XMR and TBW.

### *Convective Index Error Characteristics*

The frequency distribution of forecast PWAT is comparable during the warm season at both XMR and TBW (Figs. 12a, b). A slight conditional bias indicates that the observed PWAT is often underforecast by about 0 to 2 mm. This characteristic is confirmed in a more general sense by the overall negative (dry) forecast bias during the warm season (Table 3). The IQR varies from about 5 to 10 mm while the conditional minimum and maximum observations are distributed evenly relative to the given forecast values. Although the histogram of forecast PWAT is broader during the cool season, the character of the relationship between the forecasts and their observations remains mostly unchanged except for a reduction of the conditional dry bias (compare Figs 12a-d and Tables 3 and 4). In general, forecasts for PWAT are reliable and well refined.

Warm season lifted index forecasts are distributed from about -5 to 4 °C (Fig. 13a, b). A conditional bias is evident which suggests the forecast soundings typically have greater thermal stability than observed (i.e., forecast lifted index is greater than observed, on average). This positive bias appears in the overall sample statistics (Table 3) and was also identified previously in the form of a warm bias in the temperature error profile (QR1-98, Fig. 11). Notably, the conditional bias is smallest when the model predicts lifted indices around -3 to -4 °C. In combination with the overall stable bias, the large variability indicated by the conditional IQR and extreme observations suggest that day-to-day fluctuations in lifted index are not well represented by the meso-eta model throughout the warm season. During the cool season, the forecast lifted indices are distributed across a wider range of values (Figs. 13c, d). Since the slope of the cool season conditional median is close to that of the 45° reference line, the conditional bias remains small throughout nearly the entire given range of forecast values. Clearly, lifted index forecasts are most reliable during the cool season.

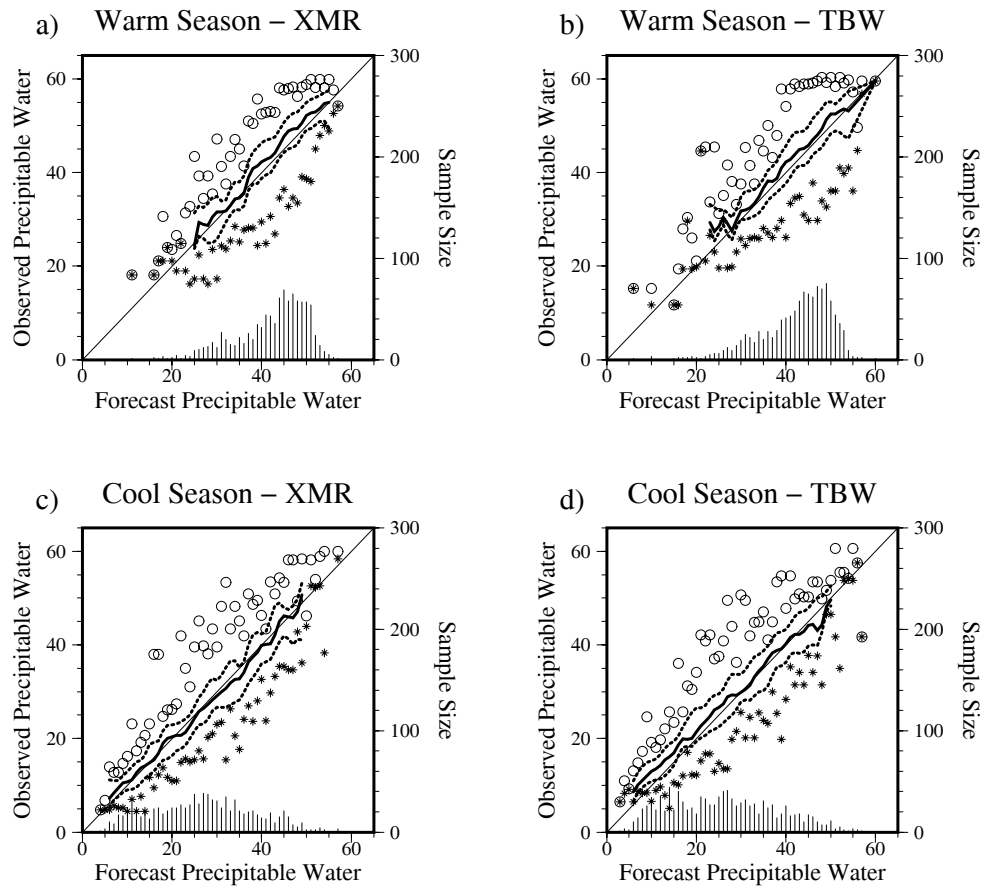


Figure 12. Quartile diagram showing the conditional distribution of observed PWAT (mm) associated with given forecast values and a histogram of the marginal distribution of forecasts. For each marginal forecast of PWAT (indicated by histogram), the minimum (maximum) observations are shown by stars (circles), the .25 and .75 quartiles are shown by dotted lines, and the .50 quartile (or median) is shown by a heavy solid line.

Table 3. Bias, RMS error and error standard deviation for warm season (May - August) convective parameters at XMR and TBW.

	Bias		RMS Error		Std. Dev.	
	XMR	TBW	XMR	TBW	XMR	TBW
Convective Index						
Precipitable Water	-1.81	-1.49	5.20	5.54	4.87	5.34
Lifted Index	1.90	1.44	3.22	2.81	2.61	2.41
K-Index	-0.37	.97	6.79	7.07	6.78	7.00
LCL	-5.63	-1.96	32.72	35.46	32.23	35.41
CAPE	-876.91	-543.34	1461.72	1104.69	1169.46	961.84
Convective Inhibition	-1.34	-9.31	65.75	63.56	65.74	62.88
Helicity	5.21	3.58	40.46	37.89	40.12	37.72
MDPI	-0.18	-0.15	.35	.31	.31	.27

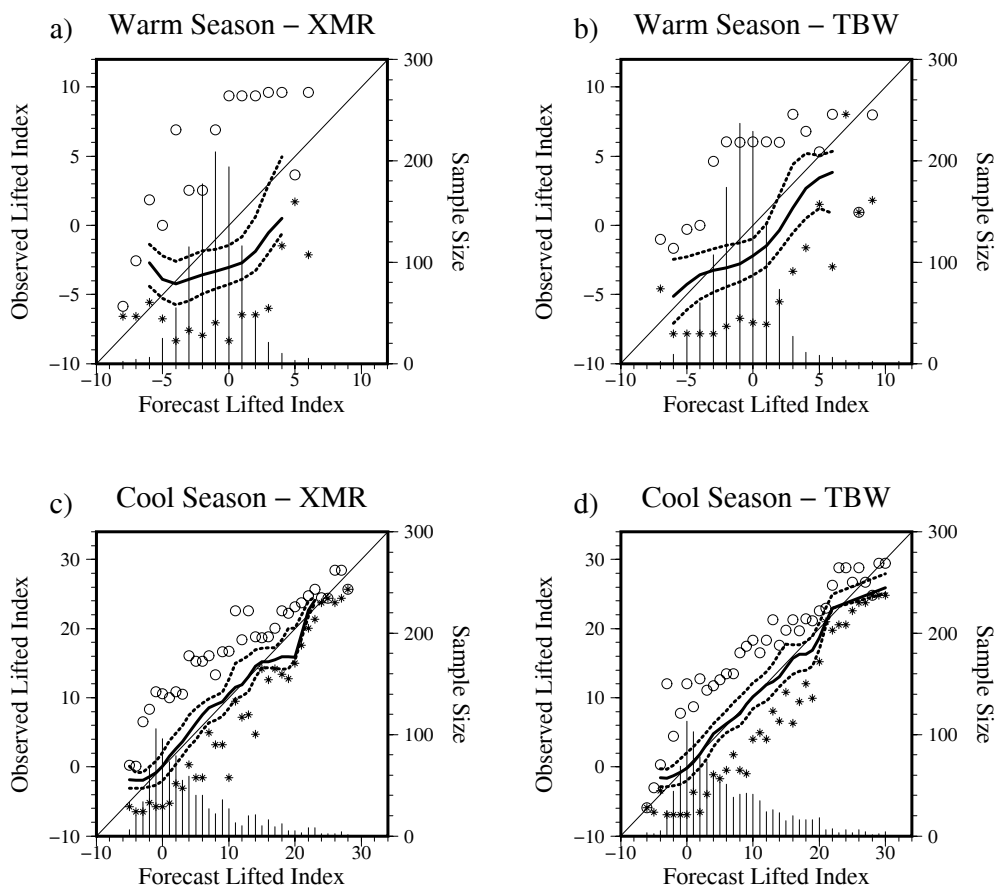


Figure 13. Quartile diagram showing the conditional distribution of observed lifted index (°C) associated with given forecast values and a histogram of the marginal distribution of forecasts. For each marginal forecast of lifted index (indicated by histogram), the minimum (maximum) observations are shown by stars (circles), the .25 and .75 quartiles are shown by dotted lines, and the .50 quartile (or median) is shown by a heavy solid line.

Table 4. Bias, RMS error and error standard deviation for cool season (October - January) convective parameters at XMR and TBW.

Convective Index	Bias		RMS Error		Std. Dev.	
	XMR	TBW	XMR	TBW	XMR	TBW
Precipitable Water	.31	-1.37	4.84	5.01	4.83	4.82
Lifted Index	-.61	-.06	2.90	2.83	2.83	2.83
K-Index	2.19	-1.24	12.11	11.29	11.91	11.22
LCL	16.58	10.64	39.53	36.65	35.88	35.07
CAPE	19.88	7.13	393.51	291.89	393.01	291.81
Convective Inhibition	1.88	2.21	32.55	47.05	32.50	46.99
Helicity	10.93	4.17	77.21	79.69	76.43	79.58
MDPI	.06	.05	.27	.24	.26	.24

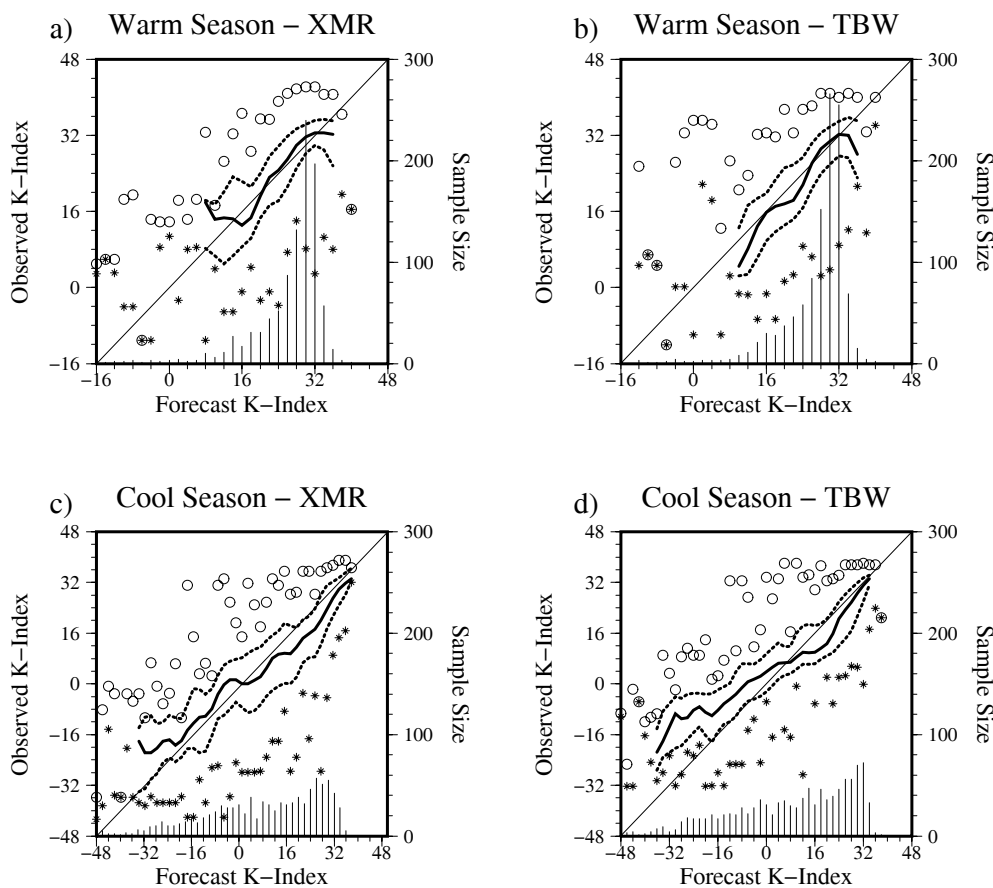


Figure 14. Quartile diagram showing the conditional distribution of observed K-index (°C) associated with given forecast values and a histogram of the marginal distribution of forecasts. For each marginal forecast of K-index (indicated by histogram), the minimum (maximum) observations are shown by stars (circles), the .25 and .75 quartiles are shown by dotted lines, and the .50 quartile (or median) is shown by a heavy solid line.

The frequency distribution of warm season K-index forecasts reveals that the indices most often lie in the range from approximately 28 to 32 °C (Figs. 14a, b). The conditional bias within this range is small, but the IQR of about

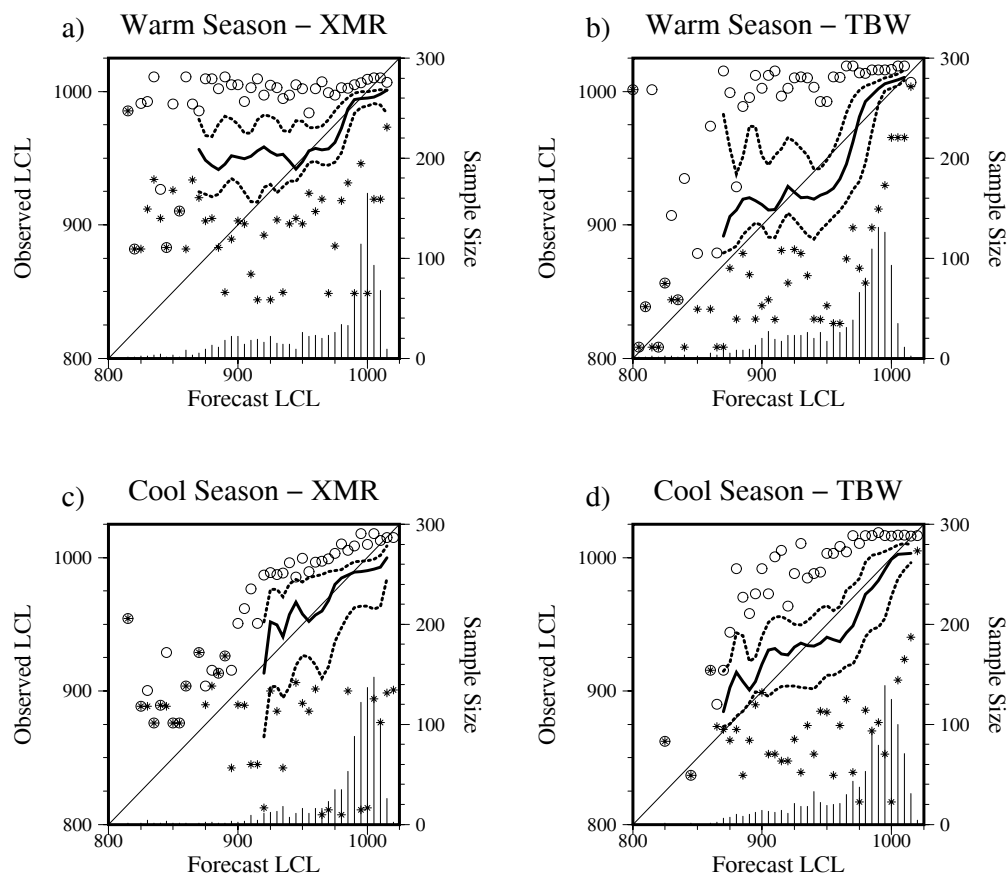


Figure 15. Quartile diagram showing the conditional distribution of observed LCL (mb) associated with given forecast values and a histogram of the marginal distribution of forecasts. For each marginal forecast of LCL (indicated by histogram), the minimum (maximum) observations are shown by stars (circles), the .25 and .75 quartiles are shown by dotted lines, and the .50 quartile (or median) is shown by a heavy solid line.

8 °C reveals substantial day-to-day variability in the forecast errors. The overall sample statistics (Table 3) also indicate that the K-index forecasts are nearly unbiased and that the error standard deviations are large in comparison to the mean. Cool season K-index forecasts are more widely distributed than the warm season forecasts (Figs. 14c, d). When cool season K-index forecasts are negative, they tend to indicate slightly greater stability than observed soundings. Conversely, when positive, the forecasts tend to indicate slightly less stability than observed.

When air parcels in the forecast soundings are lifted dry adiabatically, they most frequently reach saturation around 990 to 1000 mb during both warm and cool seasons (Fig. 15). The conditional distribution of the observed lifted condensation level (LCL) reveals that forecasts are most reliable when the LCL is closer to the ground. In particular, the large IQR and spread of extreme conditional observations reveals that LCL forecasts are less refined at lower pressures. During the cool season, the conditional median more closely follows the 45° reference line, but the distributions still exhibit a large IQR. Since subtle errors in low-level temperature and moisture will affect the calculation of forecast and observed LCL, it is not surprising that the variability is so large.

During the warm season, the forecast convective available potential energy (CAPE) distribution reveals that most forecasts contain nearly zero CAPE and thus are quite stable (Fig. 16). When warm season CAPE forecasts are less than about  $1500 \text{ J kg}^{-1}$ , the conditional median of the observed CAPE distribution is larger than the given forecast values (Figs. 16a, b). This result indicates that at smaller values, the warm season CAPE forecasts tend to underestimate the observed instability - a fact which is supported by the negative overall sample bias (Table 3). The

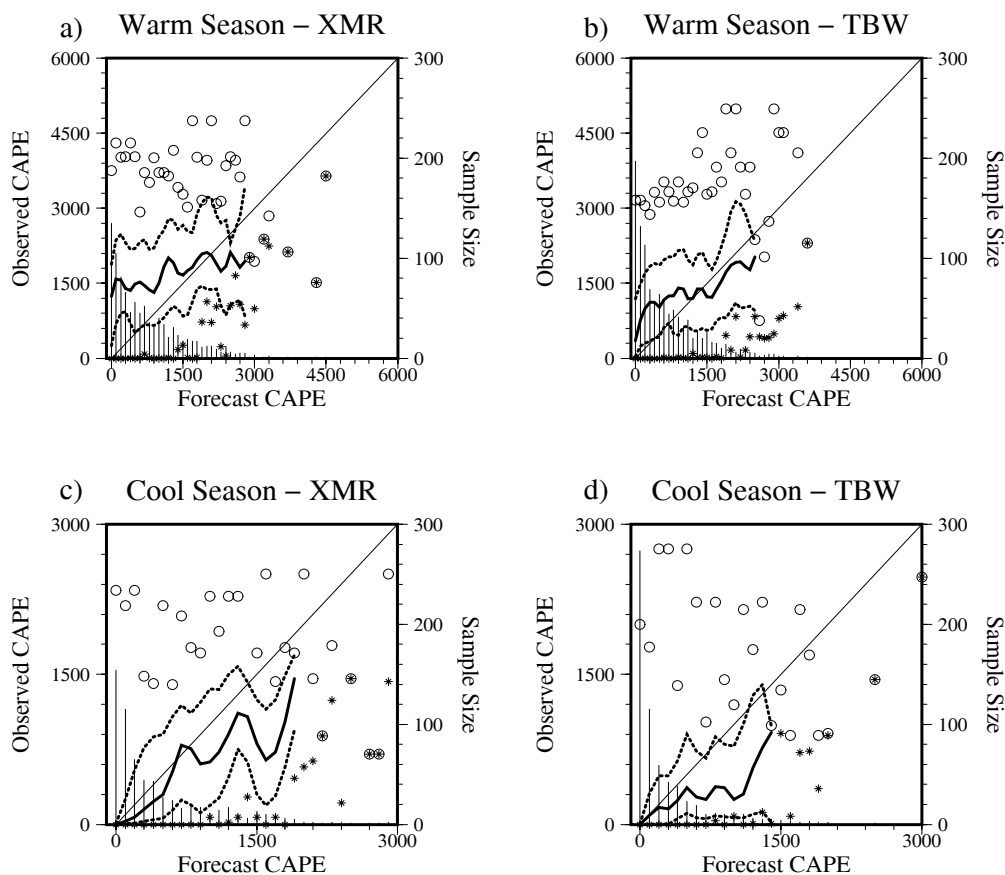


Figure 16. Quartile diagram showing the conditional distribution of observed CAPE ( $\text{J kg}^{-1}$ ) associated with given forecast values and a histogram of the marginal distribution of forecasts. For each marginal forecast of CAPE (indicated by histogram), the minimum (maximum) observations are shown by stars (circles), the .25 and .75 quartiles are shown by dotted lines, and the .50 quartile (or median) is shown by a heavy solid line.

convective potential of the forecast soundings could be limited by the positive (warm) bias in middle- and upper-tropospheric temperature (QR1-98, Fig. 11) since, in that environment, lifted air parcels would require greater energy to attain positive buoyancy. It is noteworthy that even when zero CAPE is forecast the maximum observed CAPE at XMR may exceed  $4100 \text{ J kg}^{-1}$  during the warm season ( $3000 \text{ J kg}^{-1}$  at TBW). Therefore, warm season CAPE forecasts are susceptible to large errors.

During the cool season, the frequency distribution of forecast CAPE at XMR and TBW reveals that the meso-eta model often predicts a relatively stable environment with many forecast soundings again supporting zero CAPE (Figs. 16c, d). Unlike warm season results, the cool season forecasts of small CAPE (i.e., near zero) exhibit little conditional bias and thus are reliable. However, the wide distribution of the conditional extreme observations indicates that both warm and cool season CAPE forecasts occasionally suffer large errors. Given cool season forecasts of large CAPE, a conditional bias becomes evident which suggests the environmental instability is overestimated. However, the small sample sizes associated with such forecasts decrease the credibility of this particular result.

The frequency distributions of convective inhibition (CIN) are similar to those of CAPE forecasts (compare Figs. 16 and 17). Upon first inspection, the simultaneous and regular occurrence of zero CAPE and CIN may seem in contradiction. However, the explanation is that a closed positive or negative area is not defined on a thermodynamic diagram if a lifted parcel fails to reach a level of free convection or equilibrium level within its

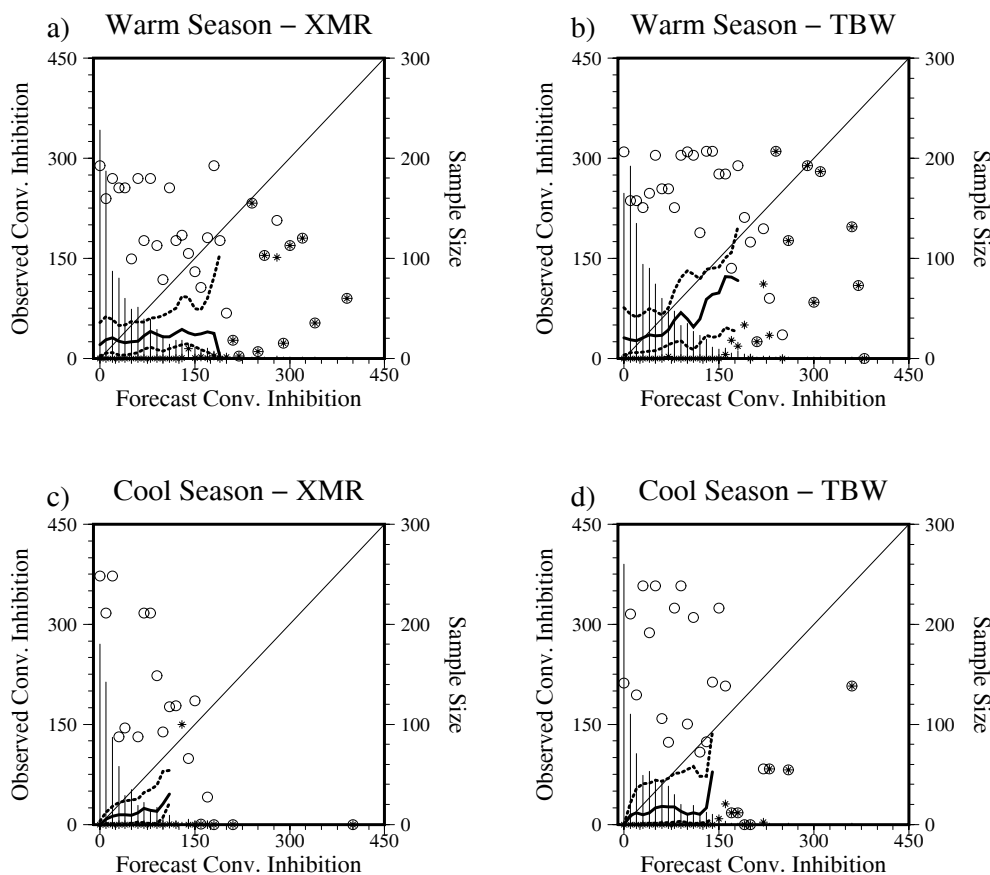


Figure 17. Quartile diagram showing the conditional distribution of observed CIN ( $J\ kg^{-1}$ ) associated with given forecast values and a histogram of the marginal distribution of forecasts. For each marginal forecast of CIN (indicated by histogram), the minimum (maximum) observations are shown by stars (circles), the .25 and .75 quartiles are shown by dotted lines, and the .50 quartile (or median) is shown by a heavy solid line.

environment. Under this circumstance, the GEMPAK numerical algorithm assigns zero CAPE and CIN to the sounding as lifted air parcels remain colder (more stable) than the environmental temperature at all levels. Examination of the warm season data from XMR (not shown) used to construct Figs. 16a and 17a reveals that instances of both zero CAPE and CIN occur in 4.9 and 2.8% of the available forecasts and observations, respectively. Similarly, 33.9 and 39.3% of the cool season forecasts and observations at XMR exhibit zero CAPE and CIN. The data for TBW demonstrate a comparable relationship. These results indicate that warm season forecasts at XMR and TBW contain zero CIN and CAPE - and are therefore stable - more often than the observed soundings. During the cool season, instances of zero CAPE and CIN occur regularly, though the observed environment is often more stable than the forecast environment.

While considering all available data, the conditional median of the observations reveals that CIN is regularly underforecast during the warm season whenever the forecast CIN is near zero (Figs. 17a, b). The fact that warm season forecasts of small (though not necessarily zero) CAPE and CIN both tend to underestimate their corresponding observations suggests that the model's boundary layer error characteristics are different from those in the free atmosphere. Indeed, the vertical profiles of temperature and mixing ratio bias (QR1-98, Figs. 11 and 12) each exhibit a shift in sign around the 700 mb level. During the cool season, the CIN forecasts are conditionally unbiased when near zero (Figs. 17c, d). This cool season reliability likely follows from the frequent occurrence of forecast and observed soundings with zero CAPE and CIN as discussed above. Given larger CIN forecasts, the

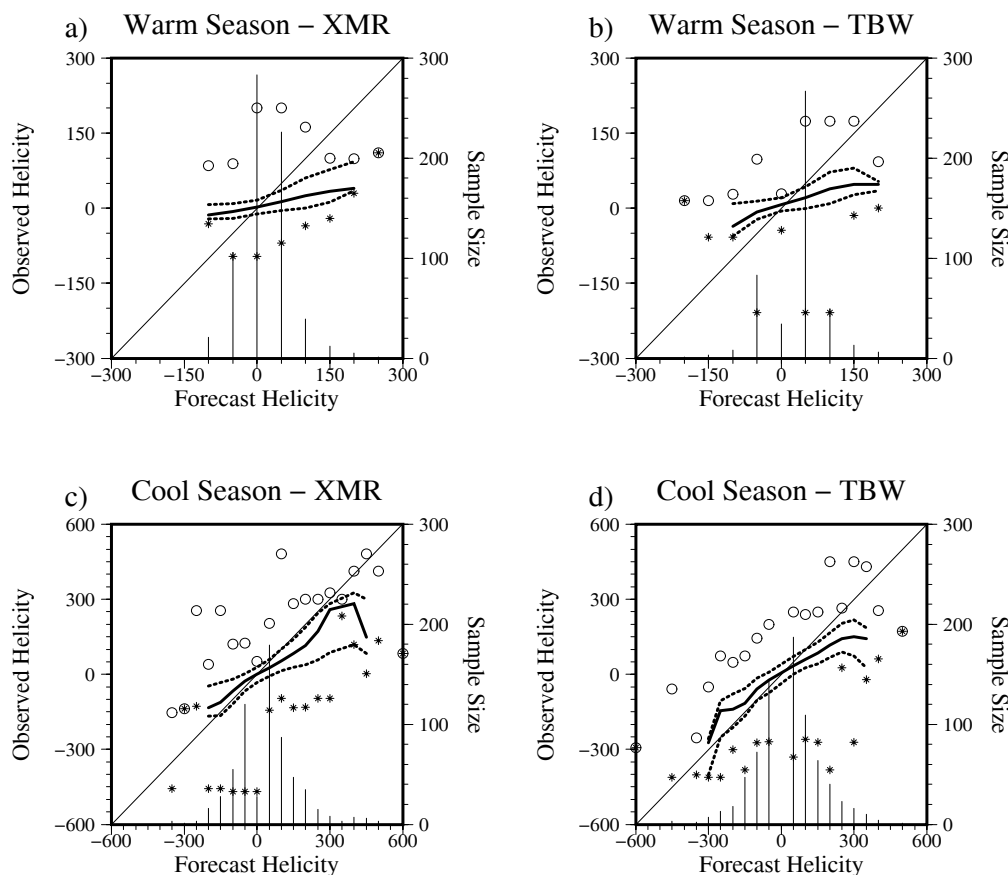


Figure 18. Quartile diagram showing the conditional distribution of observed helicity ( $m^2 s^{-2}$ ) associated with given forecast values and a histogram of the marginal distribution of forecasts. For each marginal forecast of helicity (indicated by histogram), the minimum (maximum) observations are shown by stars (circles), the .25 and .75 quartiles are shown by dotted lines, and the .50 quartile (or median) is shown by a heavy solid line.

position of the conditional median relative to the  $45^\circ$  reference line indicates that CIN is usually overforecast during both the warm and cool seasons. However, since forecasts of large CIN are relatively uncommon, this conditional bias should be considered cautiously.

Positive and negative helicity (Davies-Jones et al. 1990; Lilly 1986) forecasts are nearly evenly distributed about zero and are thus well refined during both warm and cool seasons at XMR and TBW (Fig. 18). Helicity forecasts with values near zero are conditionally unbiased. However, the lower slope of the conditional median relative to the  $45^\circ$  reference line indicates that the magnitude of the helicity is often overforecast, particularly during the warm season. The overall samples biases (Tables 3 and 4) are small but do not fully represent the tendency to overforecast the magnitude of nonzero helicity values as revealed by Fig. 18. The frequency distribution of cool season helicity forecasts covers nearly double the range of values that are forecast during the warm season. The corresponding RMS errors and error standard deviations are also approximately doubled during the cool season (Tables 3 and 4). Since helicity is a measure of the vertically integrated wind shear over the lowest 3 km of the atmosphere, the larger errors during the cool season are likely related to an increase in forecast and observed wind speeds and corresponding wind shear.

The frequency distribution for Microburst Day Potential Index (MDPI; Wheeler and Roeder 1996) forecasts indicates that most values occur in the range 0.8 to 0.9 during the warm season (Figs. 19a, b). The MDPI forecasts are conditionally unbiased and therefore reliable when near 1.0. Given MDPI forecasts less than 1.0, the potential

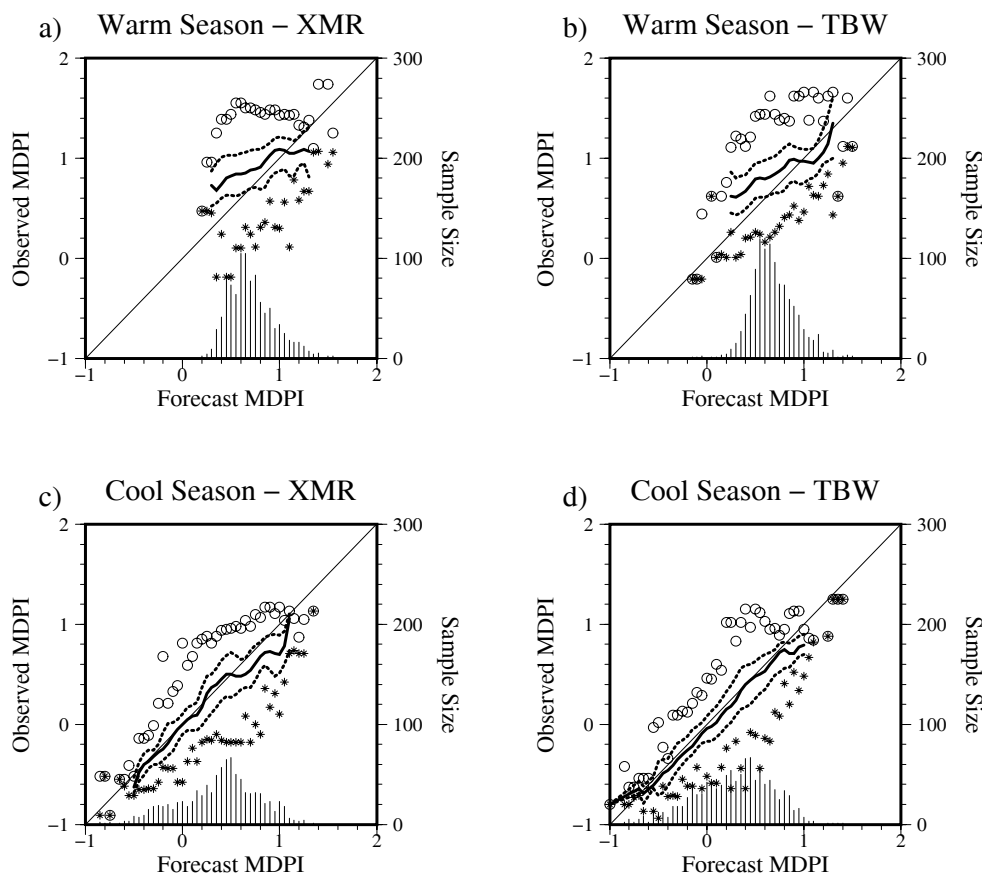


Figure 19. Quartile diagram showing the conditional distribution of observed MDPI associated with given forecast values and a histogram of the marginal distribution of forecasts. For each marginal forecast of MDPI (indicated by histogram), the minimum (maximum) observations are shown by stars (circles), the .25 and .75 quartiles are shown by dotted lines, and the .50 quartile (or median) is shown by a heavy solid line.

for microburst development is often underforecast relative to the conditional distribution of observed MDPI. Conversely, the microburst potential is typically overestimated as the forecast MDPI exceeds 1.0. Note that at XMR, the conditional maximum observed MDPI reach 1.25 across nearly the entire range of given forecast values (Fig 19a). Since MDPI values above 1.0 support a high probability of wet microburst development at XMR (Wheeler and Roeder 1996), this result suggests that the model often fails to accurately predict the environment conducive for observed microburst. The slight negative bias in the overall sample statistics (Table 3) supports the tendency to underestimate observed MDPI. During the cool season, the MDPI forecasts cover a wider range of values (more refined) while the slope of the conditional median more closely matches that of the 45° reference line (more reliable).

In general, the conditional quartile diagrams suggest that day-to-day fluctuations in observed convective indices at XMR and TBW are not well represented by the meso-eta model throughout the warm season. The forecast indices are derived from model soundings which are generally more stable than observed in the warm season. In addition, the relatively large IQR and spread between extreme values in the conditional distributions of observed indices suggest that forecasts occasionally suffer large errors in representing the true convective potential of the atmosphere. The forecast biases and variability of the errors are confirmed by the overall sample statistics (Tables 3 and 4) and support the notion that much of the error at upper levels is largely nonsystematic in nature. The index

forecasts are most refined and reliable overall during the cool season when, under normal circumstances, they provide little added value for most operational forecasting applications.

### References

- Davies-Jones, R., D. Burgess, and M. Foster, 1990: Test of helicity as a tornado forecast parameter. Preprints, 16<sup>th</sup> Conf. on Severe Local Storms, Kananaskis Park, Alberta, Canada, Amer. Meteor. Soc., 588-592.
- desJardins, M. L., S. Jacobs, D. Plummer, and S. Schotz, 1997: N-AWIPS: AWIPS at the National Centers for Environmental Prediction. Preprints, 13<sup>th</sup> International Conf. on Interactive Information and Processing Systems, Long Beach, CA, Amer. Meteor. Soc., 296-298.
- Lilly, D. K. 1986: The structure, energetics and propagation of rotating convective storms. Part II: Helicity and storm stabilization. *J. Atmos. Sci.*, **43**, 126-140.
- Murphy, A. H., B. G. Brown, and Y. Chen, 1989: Diagnostic verification of temperature forecasts. *Wea. Forecasting*, **4**, 485-501.
- Tukey, J. W. 1977: Exploratory Data Analysis. Addison-Wesley, Reading, MA.
- Wheeler, M. M., and W. P. Roeder, 1996: Forecasting wet microburst on the Central Florida Atlantic coast in support of the United States Space Program. Preprints, 18<sup>th</sup> Conf. on Severe Local Storms, San Francisco, CA, Amer. Meteor. Soc., 654-658.

### SUBTASK 7 DATA ASSIMILATION MODEL/CENTRAL FL DATA DEFICIENCY (DR. MANOBIANCO)

In the previous AMU quarterly report (First Quarter FY 98), preliminary results were presented from a warm season case study from 26-27 July 1996. The Advanced Regional Prediction System (ARPS) Data Analysis System (ADAS) was minimally configured to test its capabilities as a Local Data Integration System (LDIS) using only a single RUC background, surface observations, and NEXRAD radial velocity data. This case was selected because wind gusts exceeding 30 kt associated with an outflow boundary originating from thunderstorms to the southwest of KSC/CCAS forced Atlas launch operation A1393 to be scrubbed for the day.

In January, Dr. Manobianco presented the preliminary results of the wind analyses from the 26-27 July 1997 case at the 2nd Symposium on Integrated Observing Systems in Phoenix, AZ. Mr. Nutter also presented these results in January to SMG personnel while visiting JSC to observe weather support for the STS-89 launch. SMG provided useful feedback on the initial results using LDIS. They indicated that the 2-km rather than 10-km analyses show more utility in depicting the evolution of the thunderstorm outflow boundary for the 26-27 July case. However, the domain size of the 2-km grid (160 x 160 km centered over KSC/CCAS) is marginally adequate to help evaluate flight rules for a 90-minute landing forecast. Mr. Tim Oram emphasized that the LDIS should ultimately provide derived products that will specifically aid in the evaluation of flight rules such as cloud height/thickness and be presented using a suitable visualization package such as Vis5D.

In February, Dr. Manobianco installed and tested a new version of ADAS on the AMU's IBM RS/6000 Model 390. This latest version of ADAS was obtained from Mr. Keith Brewster at the Center for Analysis and Prediction of Storms (CAPS). Recent modifications to ADAS include the addition of a complex cloud analysis scheme and provisions to handle aircraft data, satellite-derived cloud drift and water vapor winds, and other single level data types. With these additions, ADAS now has the capability to incorporate the same data sets as FSL-LAPS for analysis.

Dr. Manobianco developed, tested, and installed software needed to reformat tower, METAR, buoy, 915-MHz and 50-MHz profiler, and RASS data into ADAS. In addition, he completed the installation and testing of software provided by CAPS to interpolate visible and infrared GOES-8 satellite data in McIDAS area files to ADAS grids. The satellite data along with surface METAR and NEXRAD data are used in the complex-cloud analysis scheme.

Dr. Manobianco and Mr. Nutter will continue with the warm and cool season case studies using the new version of ADAS to integrate all available data in central Florida and determine the potential added value of a LDIS.

#### ***2.4 AMU CHIEF'S TECHNICAL ACTIVITIES (DR. MERCERET)***

During the past quarter, Dr. Merceret continued to advise John Lane, a Ph.D. candidate at the University of Central Florida, on a study of the measurement of raindrop size distributions and their effect on Z-R relations. The work is directed at improving the use of WSR-88D and raingauge data as ground truth for NASA's TRMM project, and will serve as Mr. Lane's doctoral dissertation. It should also prove useful in using gauges to adjust or verify radar-derived rain rates, and may lead to improved NEXRAD rain rate algorithms for daily support to KSC/CCAS. Dr. Merceret completed an analysis of the effect of measurement errors in raindrop size distributions, Z and R on the calculation of Z-R relations. The results suggested some changes to Mr. Lane's use of disdrometer data currently on hand.

**NOTICE**

Mention of a copyrighted, trademarked, or proprietary product, service, or document does not constitute endorsement thereof by the author, ENSCO, Inc., the AMU, the National Aeronautics and Space Administration, or the United States Government. Any such mention is solely for the purpose of fully informing the reader of the resources used to conduct the work reported herein.

## Acronyms

45 MXS	45th Maintenance Squadron
45 WS	45th Weather Squadron
ADAS	ARPS Data Assimilation System
AMU	Applied Meteorology Unit
AMS	American Meteorological Society
ARPS	Advanced Regional Prediction System
ATDD	Atmospheric Turbulence and Diffusion Division
AWIPS	Advanced Weather Interactive Processing System
CAPE	Convective Available Potential Energy
CAPS	Center for Analysis and Prediction of Storms
CCAS	Cape Canaveral Air Station
CIN	Convective INhibition
CPM	<u>C</u> onsensus time, <u>P</u> recipitation contamination, <u>M</u> edian filter
CPW	<u>C</u> onsensus time, <u>P</u> recipitation contamination, <u>W</u> eber-Wuertz
CSR	Computer Science Raytheon
DRWP	Doppler Radar Wind Profiler
EDW	Edwards Air Force Base Rawinsonde Station Identification
ERDAS	Emergency Response Dose Assessment System
FAR	False Alarm Rate
FSL	Forecast Systems Laboratory
FSU	Florida State University
FY	Fiscal Year
GEMPAK	GEneral Meteorological PAcKage
GOES	Goestationary Orbiting Environmental Satellite
GVAR	GOES Variable
HSS	Heidke Skill Score
HYPACT	Hybrid Particle And Concentration Transport
I&M	Improvement and Modernization
IRIS	Integrated Radar Information System
IQR	Interquartile Range
JSC	Johnson Space Center
KSC	Kennedy Space Center
LAPS	Local Analysis and Prediction System
LCL	Lifted Condensation Level
LDIS	Local Data Integration System
McIDAS	Man computer Interactive Data Access System
MDPI	Microburst Day Potential Index
MFFG	Median Filter/First Guess
MSFC	Marshall Space Flight Center

---

## Acronyms

MVP	Model Validation Program
NASA	National Aeronautics and Space Administration
NCAR	National Center for Atmospheric Research
NEXRAD	NEXt-generation RADar
NGM	Nested Grid Model
NOAA	National Oceanic and Atmospheric Administration
NSSL	National Severe Storms Laboratory
NWS MLB	National Weather Service Melbourne
PC	Personal Computer
PROWESS	Parallelized RAMS Operational Weather Simulation System
PUP	Principle User Processor
PWAT	Precipitable WATer
QC	Quality Control
QR1	First Quarterly Report
RAMS	Regional Atmospheric Modeling System
RASS	Radio Acoustic Sounding Systems
REEDM	Rocket Exhaust Effluent Diffusion Model
RMS	Root Mean Square
RSA	Range Standardization and Automation
RUC	Rapid Update Cycle
RWO	Range Weather Operations
SCIT	Storm Cell Identification and Tracking
SMG	Spaceflight Meteorology Group
SNR	Signal to Noise Ratio
STS	Space Transportation System
USAF	United States Air Force
TBW	Tampa Bay area Rawinsonde Station Identification
TRMM	Tropical Rainfall Measuring Mission
VIL	Vertically Integrated Liquid
WAF	Weather and Forecasting
WATADS	WSR-88D Algorithm Testing And Display System
WSR-88D	Weather Surveillance Radar - 88 Doppler
WW	Weber-Wuertz Algorithm
WWW	World Wide Web
XMR	Cape Canaveral Rawinsonde Station Identification

## Appendix A

AMU Project Schedule 30 April 1998				
AMU Projects	Milestones	Actual / Projected Begin Date	Actual / Projected End Date	Notes/Status
Cell Trend Comparison of WATADS vs. WSR- 88D	Evaluate Effectiveness/Utility of 88D Cell Trends	Apr 97	Sep 97	Completed
	Final Report	Oct 97	Mar 98	In print - deliver in early May
SIGMET/IRIS Processor Evaluation	Evaluate SIGMET radar data manipulation and display capabilities for operational use	Jan 98	Oct 98	On schedule
	Final Report	Oct 98	Jan 99	On schedule
Boundary Layer Profilers	Wind Data Quality Objective	May 97	Jan 98	Completed
	Interim Report	Jan 98	Apr 98	1-month delay - 1 routine did not exist prior to tasking - had to develop; NASA briefing took precedence - unable to assist in writing
	Cool Season Data Collection	Nov 97	Mar 98	Ongoing
	RASS Data Quality Objective	Feb 98	May 98	1-month delay due to interim report delay
	Final Report	Apr 98	Jun 98	1-month delay
AF I&M and RSA Support	Review Document / Products, Attend Meetings / Reviews, Document Advice, Suggestions, and Comments	Jul 96	Ongoing	On schedule
Data Integration Model / Data Deficiency	Identify Mesoscale Data Sources in central Florida	May 97	May 98	On schedule
	Identify / Install Prototype Analysis System	Aug 97	Nov 97	On schedule
	Case Studies Including Data Non-incorporation	Nov 97	Jun 98	2-month delay - waiting for external data and software updates
	Final Report	Jul 98	Sep 98	2-month delay due to case studies delay

AMU Project Schedule				
30 April 1998				
AMU Projects	Milestones	Actual / Projected Begin Date	Actual / Projected End Date	Notes/Status
29-km Eta Model Evaluation Extension	Archive data for 1997/1998	May 97	Jan 98	Completed
	Perform Analysis	Sep 97	Feb 98	Completed
	Final Report	Mar 98	Apr 98	On schedule
GVAR Sounder Products Evaluation	Final Report	Jul 98	Feb 99	Proposed 2-month associated with delay in LDIS
Delta Explosion Analysis	Analyze Radar Imagery	Jun 97	Nov 97	Completed
	Run Models/Analyze Results	Jun 97	May 98	Conducting launch site climatology plan
	Final Report	Feb 98	Jun 98	
Model Validation Program	Inventory and Conduct RAMS runs for Sessions I, II, and III	Jul 97	Apr 98	Session I and III completed
	Run HYPACT for all MVP releases	Aug 97	Apr 98	Session III completed; Session I PROWESS completed
	Deliver data to NOAA/ATDD	Oct 97	Apr 98	Delayed due to delay NOAA's tape read problems
	Acquire meteorological data for Titan launches	Jul 97	Sep 98	Till end of FY98